Bergische Universität Wuppertal

Doctoral Thesis

Theoretical Molecular Spectroscopy of the Methyl Radical

Author:

Ahmad Y. Adam

Supervisor:

Per Jensen

A thesis submitted in fulfilment of the requirements

for the degree of Doctor of Philosophy

in the

Physikalische und Theoretische Chemie

Fakultät Mathematik und Naturwissenschaften

August 2018

The PhD thesis can be quoted as follows:

urn:nbn:de:hbz:468-20190828-114148-2
[http://nbn-resolving.de/urn/resolver.pl?urn=urn%3Anbn%3Ade%3Ahbz%3A468-20190828-114148-2]

DOI: 10.25926/agy6-nw67
[https://doi.org/10.25926/agy6-nw67]

Bergische Universität Wuppertal

Abstract

Faculty Name

Fakultät Mathematik und Naturwissenschaften

Doctor of Philosophy

Theoretical Molecular Spectroscopy of the Methyl Radical

by Ahmad Y. Adam

We present the first variational calculation of a room temperature *ab initio* line list for the CH_3 radical. It is based on a high level *ab initio* potential energy, dipole moment surface, and polarizability surfaces of CH_3 in the ground electronic state. The rovibrational energy levels, Einstein A coefficients, and Raman scattering coeficients were calculated variationally using the methods implemented in the computer program TROVE. Vibrational energies and vibrational intensities are found to be in very good agreement with the available experimental data. We also successfully simulated the Raman spectrum of the ν_1 fundamental band of the methyl radical as well as the $2\nu_2$ band. The first variational calculation of the isotropic hyperfine coupling constant of the carbon-13 atom in CH_3 shows that the vibrational effects constitute about 44% of the constant's equilibrium value, originating mainly from the large amplitude out-of-plane bending motion and that the temperature effects play a minor role.

Contents

List of Figures

List of Tables

Dedicated To My Parents

Chapter 1

Introduction

1.1 Spectroscopy on Free Radicals

The experimental study of free radicals started in 1900 when Moses Gomberg discovered triphenylmethyl radical. The term radical had been used in the 18th century by Antoine Lavoisier in his book Elementary Treatise of Chemistry published in 1789; but its meaning is different from the modern one. Spectroscopic observation of free radicals was not an easy task initially due to short lifetime and the lack of adequate instrumentation. Electric Discharge was a tool to produce some radicals such as methine ($CH^{\cdot}$)[1]. George Porter and others developed flash photolysis in 1950s. This invention have been applied to study the spectroscopy of free radicals with high resolution[2]. Quantum Mechanics was also an essential tool to study the spectroscopy of molecules. Herzberg was one of the pioneers of the application of quantum mechanics in spectroscopy. His work in this field were summarized by him in his a series of books termed "Molecular Spectra and Molecular Structure" with three volumes (I, II, and III). Radar research during world war II led to the developments in microwave instrumentation. This fortunately helped the development of a very important tool in the spectroscopy of radicals. In 1944, the Russian physicist Zavoisky observed the first ESR spectrum. One of the unique molecular parameters that can be obtained from ESR experiments is the hyperfine coupling constant (hfcc). The hfcc is a characteristic feature for different radical types.

In the 1960s and 1970s, Alan Carrington and his research group pioneered the application of microwave spectroscopy to a number of small-size radicals[3]. With

the development of matrix isolation techniques, infrared spectroscopy was capbale of detecting free radicals[4]. After the invention of the laser, a new powerful spectroscopic tool, laser magnetic resonance (LMR), was developed to study paramagnetic molecules. With LMR more than 100 free radicals has been detected.

1.2 Free Radicals in Space

The discovery of interstellar molecules dated back to the 1930s when the observation of optical absorption lines were assigned to diatomic radicals.

1.3 The Methyl Radical

The methyl radical is considered as one of the most important free radicals with a fundamental role in several processes. In hydrocarbon combustion processes[5], in atmospheric chemistry[6], in the chemistry of semiconductor processing[7], in the chemical vapor deposition of diamond[8], and in many chemical processes of current industrial and environmental interest. It is also present in planetary atmospheres [9], in the atmospheres of Saturn[10] and Neptune[11], and in the interstellar medium[12]. It is thought that CH_3 may be one of the most abundant free radicals in the interstellar medium[9]. Because of its central role in this variety of situations, its structural and spectroscopic parameters have been the subject of numerous studies. Different spectroscopic techniques have been devoted to determine the absolute concentration of CH_3 in the gas phase, including UV/visible[13], infrared[14], and Raman spectroscopies[15–21].

Under many experimental circumstances it is important to know the absolute concentration of a radical. This can only be carried out if accurate transition moments are available[22].

CH_3 has no permanent dipole moment, because of its D_3h symmetry. However, there is a possibility for $\Delta K{=}\pm 3$ transitions. Therefore the pure rotational transitions are dipole forbidden and very weak. And due to its planar geometry in the electronic ground state, most one-photon transitions to excited electronic states cannot be observed[23]. IR spectroscopy has become one of the most suitable

methods for its detection and it is often necessary to rely on theoretical calculations of of transition moments which cannot be always easily measured, especially in case of vibrationally excited states.

In summary, the development and application of theoretical quantitative spectroscopic predictions for of methyl radicals can benefit several fields of research.

Chapter 2

Theoretical Foundations

Nowadays, ab initio quantum mechanical calculations on small molecules can predict their structure and high-resolution spectra with high accuracy[24]. Moreover, in some cases, the theoretical prediction can offer suggestions to improve the experimental results[25, 26]. For some molecular properties, the desired accuracy required from experimental measurements is still a challenge and the aid from theoretical calculations are highly desirable, like the rovibrational transitions line intensities of molecules[27].

2.1 The Molecular Schrödinger Equation

In theoretical chemistry, the quantum mechanical calculations are based on the molecular Schrödinger equation. According to the postulates of quantum mechanics all molecular observables can be obtained by solving a suitable Schrödinger equation. For an isolated molecule with n electrons and N nuclei, the molecular Schrödinger equation in the time-independent nonrelativistic version can be written as

$$\hat{H}_{\text{molec}} \left|\Psi^{\text{molec}}_{n,v,J}(\{\mathbf{r}_i\},\{\mathbf{R}_K\})\right\rangle = E_{\text{molec}} \left|\Psi^{\text{molec}}_{n,v,J}(\{\mathbf{r}_i\},\{\mathbf{R}_K\})\right\rangle \tag{2.1}$$

where the molecular Hamiltonian, $\hat{H}_{\text{molec}}$, is

$$\hat{H}_{\text{molec}} = \frac{1}{2}\sum_{K}^{M}\frac{\hat{p}_K^2}{m_K} + \frac{1}{2m_e}\sum_{i}^{N}\hat{p}_i^2 + \frac{1}{4\pi\epsilon_0}\sum_{K<L}\frac{Z_K Z_L}{|\mathbf{R}_K - \mathbf{R}_L|} + \frac{1}{4\pi\epsilon_0}\sum_{i<j}\frac{1}{|\mathbf{r}_i - \mathbf{r}_j|} - \frac{1}{4\pi\epsilon_0}\sum_{iK}^{NM}\frac{Z_K}{|\mathbf{r}_i - \mathbf{R}_K|} \tag{2.2}$$

in which the first and second terms represents the nuclear and electronic kinetic energy, respectively. The third and fourth terms are the nuclear-nuclear and electronic-electronic potential energy terms, respectively. Finally the nuclear-electronic potential energy is represented by the fifth term.

In Eq 2.1, $|\Psi^{\text{molec}}_{n,v,J}(\{\mathbf{r}_i\},\{\mathbf{R}_K\})\rangle$ is the molecular wavefunction in terms of the electronic, $\{\mathbf{r}_i\}$, and nuclear coordinates, $\{\mathbf{R}_K\}$.

2.2 The Born–Oppenheimer Approximation

A milestone step for solving Schrödinger equation is through the Born–Oppenheimer approximation [28, 29]. Several studies investigate the breakdown of this approximation [30–37]. The approximation separates the solution of the molecular Schrödinger equation into two steps.

The electronic Schrödinger equation

$$\hat{H}_{\text{elec}}\,|\psi^{\text{elec}}_n(\{\mathbf{r}_i\},\{\mathbf{R}_K\})\rangle = E^{\text{elec}}_n(\mathbf{R}_K)\,|\psi^{\text{elec}}_n(\{\mathbf{r}_i\},\{\mathbf{R}_K\})\rangle \tag{2.3}$$

where $\hat{H}_{\text{elec}}$ is

$$\hat{H}_{\text{elec}} = \frac{1}{4\pi\epsilon_0}\sum_{K<L}\frac{Z_K Z_L}{|\mathbf{R}_K - \mathbf{R}_L|} + \frac{1}{2m_e}\sum_{i}^{N}\hat{p}_i^2 - \frac{1}{4\pi\epsilon_0}\sum_{iK}^{NM}\frac{Z_K}{|\mathbf{r}_i - \mathbf{R}_K|} + \frac{1}{4\pi\epsilon_0}\sum_{i<j}\frac{1}{|\mathbf{r}_i - \mathbf{r}_j|} \tag{2.4}$$

and the nuclear Schrödinger equation

$$\left[\frac{1}{2}\sum_{K}^{M}\frac{\hat{p}_K^2}{m_K} + E_n^{\text{elec}}(\mathbf{R}_K)\right]|\psi_{v,J}^{\text{nuc}}(\{\mathbf{R}_K\})\rangle = E_{n,v,J}^{\text{molec}}\,|\psi_{v,J}^{\text{nuc}}(\{\mathbf{R}_K\})\rangle \tag{2.5}$$

One important consequence of the the Born–Oppenheimer approximation is the concept of a potential energy surface[38] which plays a central role in many areas of chemistry, molecular structure, reaction dynamics, and spectroscopy.

2.3 The Electronic Schrödinger Equation

For the electronic Schrödinger equation 2.3, an analytical solution is difficult to find even for the simplest molecular system, the hydrogen molecular cation, H_2^+, (a quantum mechanical three-body problem). Therefore, several numerical methods have been developed to solve the electronic Schrödinger equation directly after the rise of quantum mechanics[39]. The era of using computers as a tool for computational chemistry are based on the ideas of linear combination of atomic orbitals (LCAO), basis sets, and electron correlation. This is known as the molecular orbital theory (MOT) approach in solving the electronic Schrödinger equation. However, development in an alternative approach known as Valence bond theory, is still going.

Among those methods the Hartree-Fock (HF) method[39] played an important rule. In HF method the N-electron wavefunction is represented by a single Slater determinant of N spin-orbitals. Then the eigenvalues and eigenfunctions are obtained with the application of the variational principle. The solution is based on an approximate electronic wavefunction and the difference between the Hartree-Fock energy, E_{HF}, and the true eigenvalue, E_{exact}, of the electronic Schrödinger equation is termed the 'correlation energy'

$$E_{\text{corr}} = E_{\text{exact}} - E_{\text{HF}} \tag{2.6}$$

Electronic structure calculations are based on approximating the molecular orbitals (MOs). The unknown MOs are expressed as a linear expansion in terms of a set of known mathematical functions known as basis set. Not any type of functions can be used, they should be physically reasonable. Although the Slater-type functions are more accurate, the common approach is to use Gaussian-type

functions in ab initio calculations because they are computationally more efficient with regard to two-electron integrals calculations.

For post-Hartree-Fock electronic structure calculations, a type of basis sets have been developed by Dunning and co-workers known as correlation consistent basis sets. This type of basis functions has been employed in our work here in building the PES and in computing electric and magnetic molecular properties[39].

To account for the correlation energy Eq. 2.6, many electron correlation methods have been developed. The goal is a better description of the correlation effect than the one provided by Hartree-Fock methods. For the electron correlation methods currently exists there is no ultimate choice for a specific method and this will depends on the question in hand and the type of molecule under study, for example an open-shell or a closed-shell molecule. In other words, different methods for different applications is the common way in the literature.

The configuration interaction (CI) treatment of electron correlation is one of the earliest approaches. The CI wave function is built as a linear combination of excited Slater determinants (configurations) and the expansion coefficients are determined according to the variational principle. A perfect trial CI wavefunction would be a type of full configurations. However, due to computational efficiency, the CI wavefunction is truncated to certain excitation orders. The acronyms CIS, CISD, CISDT would refer to truncated CI wavefunctions with linear combination up to singly, doubly, and triply excited determinants, respectively[39].

Based on perturbation theory, the Møller-Plesset (MP) treatment of electron correlation is one approach developed in 1934 and the most popular version of it is the second-order Møller-Plesset perturbation theory (MP2)[39].

A very successful method in the treating the electron correlation problem is the coupled-cluster (CC) method. In analogues fashion to CI methods, with regard to the idea of generating the correlated wavefunction in terms of an expansion of excited determinants is repeated here. The trunction of the expansion would similarly produce CCSD, CCSDT, etc methods in the CC family. However, the form of the expansion in CC methods is different from the one used in CI methods. One of the methods, CCSD(T), has been termed the gold standard of Quantum Chemistry[39].

To conclude this section, we have discussed three types of correlated wavefunction-based methods. In our work in chapters 3, 4, and 5 we have applied the CCSD(T) method with the UHF as a reference. The type of basis set we have employed is of the correlation-consistent type. With electronic structure calculations, we have computed the potential energy surface and the associated molecular properties (hyperfine coupling constant, dipole moment, and polarizability surfaces). More details are in the following chapters.

2.4 The Nuclear Schrödinger Equation

Nuclear motion calculations is now a mature field and the level of development that has been achieved in solving of the nuclear Schrödinger equation has been termed the "fourth age of quantum chemistry"[40]. Several methods have been developed from the Rigid-Rotor Harmonic Oscillator basic model to advanced models with perturbation and variational approaches[41].

2.4.1 Rigid-Rotor Harmonic Oscillator

A primitive and important model for vibration–rotation spectroscopy is based on the harmonic-oscillator and rigid-rotor approximations. Molecular vibrations are independent normal modes. The equilibrium bond length do not change when the molecule rotates, a rigid body. With second derivatives of the electronic energy with respect to the variations in nuclei positions we form the molecular Hessian. Upon diagonalizing of this force constant matrix, harmonic frequencies are obtained. This is available for quantum-chemical methods like HF, MP2, and CCSD(T).

This model is useful as a starting point and contribute a large part of the rovibrational energies but it can not be applied for real-life problems in spectroscopy and more advanced methods are needed.

2.4.2 Vibrational Pertrubation Theory

A successful approach to solve the nuclear Schrödinger equation for semi-rigid molecules with small amplitude motions is the second-order vibrational Perturbation Theory (VPT2)[42–46]. A extension to a fourth-order (VPT4) has been developed and applied to equilibrium molecular structure [47] and transition state theory[48].

In cases when resonance is present second-order vibrational perturbation theory is not a appropriate choice. And generally, it is not adequate for vibrationally excited states and large-amplitude motions. The variational approach is more applicable in treatment of such cases.

2.4.3 Variational Methods

The general steps in variational calculations[49] are

(1) Specify a coordinate system.
(2) Determine the form of the kinetic energy operator.
(3) Calculate the ab initio Born-Oppenheimer potential energy surface.
(4) Fit the obtained PES to a suitable function
(5) Choose a set of basis functions to represent the Hamiltonian as a matrix.
(6) Calculate the matrix elements.
(7) Diagonalize the Hamiltonian matrix.

To compute Infrared or Raman intensities two additional steps are required

(8) Compute the ab initio dipole moment surface and fit it to an appropriate function

(9) Compute the ab initio polarizability surface and fit it to an appropriate function

The variational approach is more accurate than perturbative approach but it is computationally more expensive.

2.4.3.1 Semi-rigid treatments

Based on the Watson Hamiltonian, variational approaches to compute the vibrational energies of polyatomic molecules have been developed[50]. The methodology

is similar to those methods developed to solve the electronic Schrödinger equation. The vibrational wavefunction can be represented as a Hartree product and a self-consistent-field can be performed, the so-called vibrational self-consistent-field (VSCF) method. The VSCF method to include correlation can be extended to vibrational configuration interaction (VCI) [50] and vibrational coupled-cluster (VCC) methods[51].

This variational approach is limited to near-equilibrium structure for polyatomic molecules and is not suitable for large amplitude motions. The rotational part is not included either; however, a recent attempt has been made to apply a rovibrational Hamiltonian at the second order vibrational Møller–Plesset perturbation theory (VMP2)[52]

2.4.3.2 Large Amplitude Motions

The treatment of large amplitude motions (LAM) in polyatomic molecules with variational methods is described in section 2.5.

2.5 TROVE

Theoretical ROVibrational Energies (TROVE) [53–57] is a computer program developed to compute rovibrational energies and the associted molecular properties (IR intensities, Raman scattering cross sections, vibrational effects on molecular properties, etc)

2.5.1 Potential Energy Function

Based on the Born-Oppenheimer approximation to construct the rovibrational Hamiltonian, we need to build the molecular potential energy hypersurface or simply the potential energy surface (PES). One way to build the PES in which the nuclear motion can vibrate and rotate can be obtained by solving the electronic Schrodinger equation (section 2.3) in series of caluclations for a set of molecular geomteries. Each calculation represents a unique geometry of the molecule under study. The produced data from these computations will be fitted in a functional form in a final step to represent the PES.

The analytical function of PES is expressed in terms of pre-defined internal coordinates, ξ_i. For example, the calculated points of the potential energy surface of CH_3 in the electronic ground state is fitted to a totally-symmetric sixth-order power series expansion in terms of six variables

$$\begin{aligned}
\xi_k &= (r_k - r_e)\exp\left(-(r_k - r_e)^2\right), \quad k = 1, 2, 3, && (2.7)\\
\xi_4 &= (2\alpha_1 - \alpha_2 - \alpha_3)/\sqrt{6} && (2.8)\\
\xi_5 &= (\alpha_2 - \alpha_3)/\sqrt{2} && (2.9)\\
\xi_6 &= 1 - 2/\sqrt{3}\sin([\alpha_1 + \alpha_2 + \alpha_3]/6) && (2.10)
\end{aligned}$$

where $r_k - r_e$ denotes the displacement from the equilibrium value r_e of the distance between C and H_k, α_1, α_2, and α_3 are the instantaneous values of the bond angles $\angle(H_2\text{–}C\text{–}H_3)$, $\angle(H_1\text{–}C\text{–}H_3)$, and $\angle(H_1\text{–}C\text{–}H_2)$, respectively.

2.5.2 The Kinetic Energy Operator

The second essential part in our soultion of the nuclear Schrodinger equation in molecular spectroscopy is a proper form for the Hamiltonian in terms of the kinetic energy operator (KEO) within the Eckart conditions[58]. To construct the KEO, we need to choose a suitable coordinate system. There are two main types of coordinates, Cartesian and internal coordinates.

The KEO has a very simple form in terms of the Cartesian coordinates.

$$\hat{T} = \frac{1}{2}\sum_{F=X,Y,Z}\sum_{i=1}^{N}\frac{\hat{P}_{iF}^2}{m_i} \qquad (2.11)$$

where $\hat{P}_{iF}$ $(i = 1 \ldots N,\ F = X, Y, Z)$ is the momentum conjugate to the Cartesian coordinate R_{iF} (R_{iX}, R_{iY}, R_{iZ}) in the chosen laboratory-fixed axis system XYZ.

Inspite of the simplicity of Eq. 2.11, it does not allow us to distinguish between the different types of nuclear motion, the translational, vibrational, and rotational motions. In order to separate these motions and treat them independently in case of weak coupling we need to transforn to a suitable type of coordinate system.

The goal is to express the nuclear Hamiltonian in terms of $3N$ new generalized coordinates

$$\boldsymbol{\Xi} = (R_X^{\mathrm{CM}}, R_Y^{\mathrm{CM}}, R_Z^{\mathrm{CM}}, \theta, \phi, \chi, \xi_1, \xi_2, \ldots, \xi_{3N-6}). \tag{2.12}$$

The translational motion is described by three coordinates; where R_F^{CM} ($F = X$, Y, Z) is the F-coordinate of the nuclear center of mass; To define the orientation of the xyz axis system relative to the XYZ system, we use the Euler angles (θ, ϕ, χ)[59]. This will describe the over-all rotation of our molecular system. Finally, the vibrational motion is described by the internal coordinates ξ_n.

Another useful definition to facilitate the transformation of the kinetic energy operator $\hat{T}$ to a new coordinate system is the generalized momenta

$$\hat{\boldsymbol{\Pi}} = (\hat{P}_X^{\mathrm{CM}}, \hat{P}_Y^{\mathrm{CM}}, \hat{P}_Z^{\mathrm{CM}}, \hat{J}_x, \hat{J}_y, \hat{J}_z, \hat{p}_1, \hat{p}_2, \ldots \hat{p}_{3N-6}), \tag{2.13}$$

where $\hat{P}_F^{\mathrm{CM}}$ ($F = X, Y, Z$) is the momentum conjugate to the translational coordinate R_F^{CM}, $(\hat{J}_x, \hat{J}_y, \hat{J}_z)$ are the xyz components of the total angular momentum,[59] and $\hat{p}_n = -i\hbar\partial/\partial\xi_n$ ($n = 1, \ldots, 3N-6$) is the momentum conjugate to the vibrational coordinate ξ_n.

The transformation from generalized momenta Π_λ to the Cartesian conjugate momenta P_{iF} ($i = 1..N$, $F = X, Y, Z$), is defined by

$$P_{iF} = \sum_{\lambda=1}^{3N} s_{\lambda,iF}\, \Pi_\lambda, \tag{2.14}$$

where $s_{\lambda,iF}$ is a Jacobian matrix with elements

$$s_{\lambda,iF} = \frac{\partial q_\lambda}{\partial R_{iF}}. \tag{2.15}$$

The rovibrational kinetic energy can be written as [60]:

$$T = \frac{1}{2} \sum_{i=1}^{N} \sum_{F=X,Y,Z} m_i^{-1}\, P_{iF} P_{iF} = \frac{1}{2} \sum_{\lambda=1}^{3N} \sum_{\mu=1}^{3N} \Pi_\lambda\, G_{\lambda,\mu}\, \Pi_\mu, \tag{2.16}$$

where

$$G_{\lambda,\mu} = \sum_{\alpha=x,y,z} \sum_{i=1}^{N} \frac{s_{\lambda,i\alpha} s_{\mu,i\alpha}}{m_i}. \tag{2.17}$$

Now, the matrix elements $s_{\lambda,i\alpha}$ define the expression for the kinetic energy in terms of the momenta conjugate to the generalized coordinates $\boldsymbol{\Xi}$.

The form of Eq. 2.15 is unknown and to find a solution we assume that the square matrix with elements $s_{\lambda,iF}$ can be represented with the chain rule:

$$\sum_{i=1}^{N} \sum_{F=X,Y,Z} \frac{\partial \Xi_\lambda}{\partial R_{iF}} \frac{\partial R_{iF}}{\partial \Xi_\mu} = \delta_{\lambda,\mu}, \tag{2.18}$$

or

$$\sum_{i=1}^{N} \mathbf{s}_{\lambda,i} \cdot \mathbf{t}_{i,\mu} = \delta_{\lambda,\mu}. \tag{2.19}$$

With the definition

$$t_{iF,\mu} = \frac{\partial R_{iF}}{\partial \Xi_\mu}, \tag{2.20}$$

where the vectors $\mathbf{t}_{i,\mu}$ have the XYZ coordinates $(t_{iX,\mu}, t_{iY,\mu}, t_{iZ,\mu})$.

An analytical solution of equation 2.19 is not feasible. If the $\mathbf{t}_{i,\mu}$-vectors are known, a numerical solution can be preformed. Therefore, by solving Eq.(2.19) via numerical techniques, we can obtain the $\mathbf{s}_{\lambda,i}$-vectors. The xyz coordinates of the $\mathbf{t}_{i,\lambda'}$-vectors are given as [61]

$$\begin{array}{lcll} t_{i\alpha,\alpha'} & = & \delta_{\alpha,\alpha'} & \text{(translation)} \\ t_{i\alpha,\beta} & = & \sum_\gamma \epsilon_{\alpha\beta\gamma} R_{i\gamma}^{\mathrm{MS}} & \text{(rotation)} \\ t_{i\alpha,n} & = & \partial R_{i\alpha}^{\mathrm{MS}} / \partial \xi_n & \text{(vibration).} \end{array} \tag{2.21}$$

To summarize this subsection, obtaining $\mathbf{t}_{i,\mu}$ numerically will produce $s_{\lambda,iF}$. This will give us $G_{\lambda,\mu}$ in Eq. 2.17 and finally we will obtain the KEO in a new form.

2.5.3 Basis Functions

The next step in the variational method after building the PES and constructing the KEO is to choose a set of basis functions to represent the Hamiltonian as a matrix. Then finally calculating the matrix elements and diagonalizing the Hamiltonian to obtain the eigenvalues (rovibrational energies) and eigenfunctions.

The rigid symmetric rotor wavefunctions $|J, k, m\rangle$ are the usual representation of the rotational basis set [59]. The quantum numbers J, k, and m are associated with the total angular momentum, its projection onto the z axis of the molecular axis frame and its projection onto the Z axis of the laboratory axis frame, respectively.

The harmonic oscillator basis functions can be used as a candidate for the bending motions in molecules.

For stretching vibrational motion, a harmonic oscillator function could be a candidate. However, the PES of diatomic molecules as well as polyatomic molecules can be better described by Morse basis functions. The Morse potential

$$V_{\text{Morse}}(r) = D\, y^2 = D\, \left[1 - \exp(-a\Delta r)\right]^2 \tag{2.22}$$

In equation (2.22), r is the internuclear distance describing the stretching motion and $\Delta r = r - r_e$ is the displacement from the equilibrium value r_e, D is the dissociation energy, a is a parameter determining the curvature of the potential at $r = r_e$, and $y = 1 - \exp(-a\Delta r)$.

A Morse potential has favorable properties with regard to good convergence and simple expressions for matrix elements.

2.5.4 Computational steps

Obtaining theoretical rovibrational intensities with TROVE consists of the following computational steps:

1. Solution of the vibrational problem
   (a) Construction of the Hamiltonian (in terms of the internal coordinates)
      - Expansion of the kinetic energy term
      - Expansion of the potential energy function
      - Expansion of the electric dipole function (or any other property)
   (b) Construction of starting vibrational basis sets
      - Solution of the 1D Schrödinger equations.
      - Solutions of the reduced Hamiltonian problems.

- Construction of the symmetry-adapted vibrational basis set.

(c) Calculation of the matrix elements for

- The vibrational part of the Hamiltonian operator
- The dipole moment function.

(d) Diagonalizaitons of the vibrational Hamiltonian matrices

- for each irreducible representation

2. Solution of the rovibrational problem

(a) Construction of the rovibrational basis set (as a direct product of)

- the J=0 eigenfunctions
- and rigid-rotor wavefunctions

(b) Construction of the rovibrational Hamiltonian matrices

- for each $J \geq 0$ and irreducible representation Γ

(c) Diagonalizations of the Hamiltonian matrices

3. The intensity calculations,

- Each pair of the rovibrational eigenvectors from Step 2c are correlated with the dipole moment XYZ components
- The correlation is restricted to the selection rules.
- The body-fixed xyz components of the dipole moment from Step 1c are transformed to the XYZ-frame using the Wigner-matrices.

FIGURE 2.1: TROVE algorithm

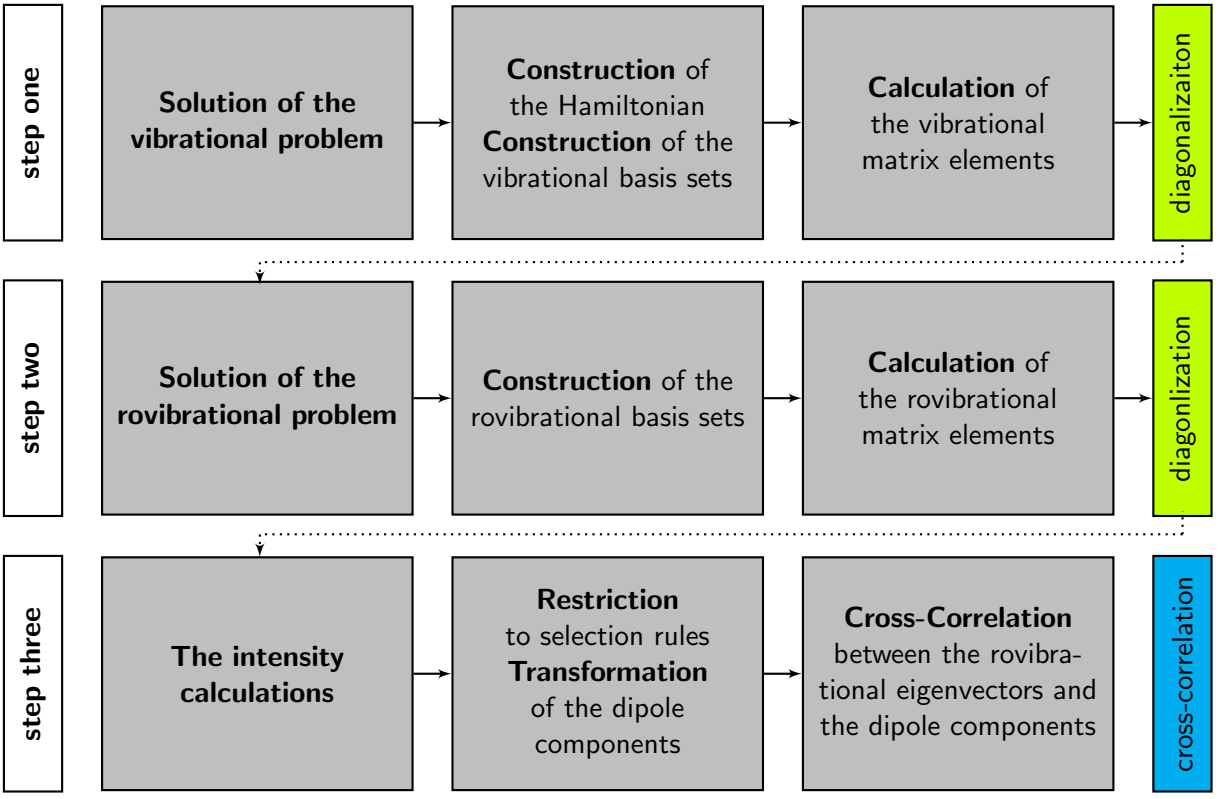

Chapter 3

ESR – Hyperfine structure

*

We present the first variational calculation of the isotropic hyperfine coupling constant of the carbon-13 atom in the CH_3 radical for temperatures T = 0, 96, and 300 K. It is based on a newly calculated high level ab initio potential energy surface and hyperfine coupling constant surface of CH_3 in the ground electronic state. The rovibrational energy levels, expectation values for the coupling constant, and its temperature dependence were calculated variationally by using the methods implemented in the computer program TROVE. Vibrational energies and vibrational and temperature effects for coupling constant are found to be in very good agreement with the available experimental data. We found, in agreement with previous studies, that the vibrational effects constitute about 44% of the constant's equilibrium value, originating mainly from the large amplitude out-of-plane bending motion and that the temperature effects play a minor role

3.1 Introduction

The importance of the nuclear motion contributions to various electromagnetic molecular properties is by now well understood. [62–80] The zero-point vibrational corrections (ZPVC) are proved to be non-negligible for the electron paramagnetic resonance (EPR)[79, 81], nuclear magnetic resonance (NMR) [69, 76, 82]

*Reproduced from J. Chem. Phys., 143:244306/1–7, 2015, with permission of the AIP Publishing

and non-linear optical (NLO) properties. [70, 83] The so-called pure vibrational contributions to NLO properties [84] are often comparable or even larger in magnitude than that due to electronic motions[64, 65, 70–72]. Moreover, some of the experimentally observed effects, such as temperature dependence and isotope shifts of electric and magnetic properties are entirely due to the effect of molecular vibrations and rotations. [76]

Several successful methods for evaluating the rovibrational contributions to various molecular properties were formulated using the perturbation theory (PT) approach over the last few decades [66, 67, 85, 86]. The applications of the PT-based approaches are however limited to quasi-rigid molecules vibrating harmonically within a single minimum potential energy surface (PES). For molecules exhibiting large amplitude anharmonic motions, due to the poor convergence of the PT expansion, the rovibrational wave functions and subsequent contributions to molecular properties must be obtained by variational methods. This, however, is much more computationally demanding and requires a more sophisticated numerical description of the PES. Thus, it is only applicable to small molecules. Only recently a few general variational methods have been proposed capable of solving the rovibrational problem accurately for very highly excited states. These methods are routinely applicable to molecules with an arbitrary geometrical structure[54, 55, 87–89]. One of them, TROVE,[54, 55] has been applied to compute the ZVPC-, temperature-, and isotope-dependence of the isotropic spin-spin coupling constants of NH_3[76]. The response theory approach has been developed for the vibrational configuration interaction method allowing accurate calculations of the pure vibrational contributions to the NLO properties[90, 91]. In these and a few other [71, 78, 80] studies, the importance of a proper variational treatment of the large amplitude vibrations in obtaining accurate estimates of molecular properties has been emphasized.

In the present work we report the first comprehensive variational calculations of the rovibrational contributions to the isotropic hyperfine coupling constant of the carbon-13 atom in the methyl radical CH_3, which we henceforth refer to as HFCC. The methyl radical is important in combustion processes and as an intermediate in many chemical reactions, [92] it has been observed in interstellar space, [9] and it is an example of a molecule with large vibrational contribution to HFCC that accounts for up to about 41% of the total value.[79] CH_3 has been the subject of many theoretical studies [93–104] characterizing the electronic structure and

vibrational motion. The most recent works [103, 104] reported the *ab initio* calculated PES and dipole moment surface and the variational rovibrational energy calculations for CH_3. Also, there have been a number of theoretical studies of the HFCC for $^{13}CH_3$[79, 105–107]. To the best of our knowledge, in all previous studies of the HFCC the vibrational effects were described by means of PT. In the present work, we have computed the new PES and HFCC surface for CH_3 in the ground electronic state.

For the PES we used the explicitly correlated coupled cluster CCSD(T)-F12 level [108] with the correlation consistent basis set cc-pVQZ-F12, [109] while the HFCC was computed by means of the conventional CCSD(T) with the augmented correlation consistent basis set aug-cc-pVTZ-J [110, 111]. We expect these methods to yield an adequate accuracy for at least low energy levels, sufficient to converge the rovibrational contributions to HFCC at the room temperature and below. The PES and HFCC surfaces were used to compute the rovibrational energy levels, ZPVC, and temperature corrections to HFCC by means of the variational method TROVE[54, 55]. The resulting vibrational energies and total value of the HFCC at a temperature $T = 96$ K were found to be in good agreement with experiment, as well as with results of previous theoretical studies. For illustrative purposes we compared the variationally computed expectation values of HFCC with those obtained from the perturbed-rigid-molecule (PRM) approach. As expected, the results confirm that PRM is not reliable for the expectation values of CH_3 in the excited out-of-plane bending states.

3.2 Computational Details

The calculations of the HFCC have been carried out within the framework of the Born-Oppenheimer approximation following a conventional three-step approach. First, the *ab intito* calculations of the ground state potential energy surface and the electronic contribution to HFCC are performed, which are followed by the calculations of the rovibrational energy levels and wave functions. The HFCC values associated with the rovibrational states of interest or their Boltzmann distribution are evaluated by averaging the *ab initio* HFCC function over the corresponding rovibrational wave functions.

3.2.1 Electronic structure calculations

The electronic energies for the ground electronic state of CH_3 were computed on a grid of 22 640 symmetry-unique molecular geometries employing the open-shell RCCSD(T)-F12b [108, 112] level of theory (explicitly correlated F12 restricted coupled cluster included single and double excitations with a noniterative correction for triples) and the F12-optimized correlation consistent polarized valence basis set cc-pVQZ-F12 [109]. In correlated calculations the carbon inner-shell electron pair was treated as frozen core. The diagonal fixed-amplitude ansatz 3C(FIX) [113] and a Slater geminal exponent value of β=1.0 (Ref.[114]) were used. To evaluate the many-electron integrals in F12 theory, three additional auxiliary basis sets are required. For the resolution of the identity basis and the two density fitting basis sets, we utilized the corresponding OptRI,[115] cc-pV5Z/JKFIT,[116] and aug-cc-pwCV5Z/MP2FIT [117] basis sets, respectively. Calculations were carried out using the MOLPRO program [118]. The analytical representation for the PES was obtained in a least-squares fitting procedure using the functional form from Ref.[119]. By varying 248 parameters we achieved a fitting root-mean-square deviation (rms) of 0.9 cm^{-1}. The values of the fitted parameters are given in the supplementary material [120] together with a Fortran 90 routine for calculating the PES.

For the coupling-constant surface, the geometry-dependent values of the isotropic hyperfine coupling constant (also known as Fermi contact term) for carbon were obtained[†] as, see Appendix A,

$$A_{\mathrm{iso}}^{(N)} = \frac{2}{3}\mu_0\,\mu_{\mathrm{N}}\,g_{\mathrm{N}}\,\rho(N) \tag{3.1}$$

for 19 959 symmetry-unique molecular geometries.

In Eq. (3.1), the index N labels a specific nucleus (carbon in our case), μ_0 is the vacuum permeability, μ_{N} is the nuclear magneton, g_{N} is the nuclear g factor, and $\rho(N)$ is the spin density at the carbon nucleus. The hyperfine coupling constant is an important parameter in EPR spectroscopy; it describes the hyperfine splitting and structure of an observed spectrum. A non-vanishing HFCC is due to

[†]In units of T (tesla) when all quantities on the right hand side of Eq.(3.1) are in SI units; another customary unit is the Gauss (G); 1G = 10^{-4} T.

interaction between the magnetic moments of the unpaired electron and the nuclei in the molecule. It is usually reported in the literature in units of magnetic field strength (G or T) required to produce the resonance condition. To obtain the HFCC in Hz, the right hand side of Eq. (3.1) should be multiplied by the conversion factor $g_e\mu_B/h$ (Hz T^{-1}), where g_e is the g-factor of free electron, μ_B is the Bohr magneton, and h is the Planck constant. In the static view of CH_3 as a planar molecule, there is no direct contribution from the unpaired electron to the HFCC and the main contribution comes from spin polarization effects. The out-of-plane vibration allows and adds the direct contribution from the unpaired electron to the equilibrium value of the HFCC.

We have calculated the HFCC employing the all-electron unrestricted open-shell CCSD(T) level of theory to account for spin polarization effects and the basis set aug-cc-pVTZ-J [110, 111] designed to ensure the proper nuclear-cusp behaviour of the electronic wave function and thus a good description of the HFCC. The calculations were performed with the CFOUR program. [121] We have fitted the calculated points to the totally-symmetric sixth-order power series expansion [122] in terms of six variables

$$\xi_k = (r_k - r_e)\exp\left(-(r_k - r_e)^2\right), \quad k = 1,2,3, \tag{3.2}$$

$$\xi_4 = (2\alpha_1 - \alpha_2 - \alpha_3)/\sqrt{6} \tag{3.3}$$

$$\xi_5 = (\alpha_2 - \alpha_3)/\sqrt{2} \tag{3.4}$$

$$\xi_6 = 1 - 2/\sqrt{3}\sin([\alpha_1 + \alpha_2 + \alpha_3]/6) \tag{3.5}$$

where $r_k - r_e$ denotes the displacement from the equilibrium value r_e of the distance between C and H_k, α_1, α_2, and α_3 are the instantaneous values of the bond angles $\angle(H_2\text{–}C\text{–}H_3)$, $\angle(H_1\text{–}C\text{–}H_3)$, and $\angle(H_1\text{–}C\text{–}H_2)$, respectively. The factor $\exp(-(r_k - r_e)^2)$ in Eq. (3.2) ensures a physically reasonable asymptotic behaviour of the power series at large distances r_k[123]. In a least-squares fitting procedure we determined 185 expansion parameters that reproduce the HFCC data with the rms of 0.11G. The optimized parameters together with the Fortran 90 function for calculating the HFCC surface are given in the supplementary material[120].

3.2.2 Nuclear Motion Calculations

The *ab initio* PES was used to compute the rovibrational energy levels of CH_3 employing the variational approach and computer program TROVE[54, 55]. In TROVE the rovibrational Hamiltonian is defined by the power-series expansions of its kinetic energy (KEO) and potential energy (PES) operators in terms of internal coordinates around the equilibrium or reaction-path configuration. In the present work the expansions of the kinetic and potential parts were truncated after the 6-th and 8-th order terms, respectively, and the six internal coordinates are: three r_i = C–H_i ($i = 1..3$) stretching coordinates, two symmetry-adapted bending coordinates ξ_4 and ξ_5, as given in Eqs. (3.4,3.5), and one out-of-plane bending coordinate τ (see Ref.[124] for details). The size of the vibrational basis set is controlled by the polyad number P

$$P = 2(n_{r_1} + n_{r_2} + n_{r_3}) + n_{\xi_4} + n_{\xi_5} + n_\tau/2 \tag{3.6}$$

where n_i are the quantum numbers defined in connection with the primitive basis functions,[54] each describing i-th vibrational degree of freedom. They are essentially the principal quantum numbers associated with the local mode vibrations of CH_3. The vibrational basis set contains only products of primitive functions for which $P \leq P_{\max}$. We found that $P_{\max} = 10$ was sufficient to converge the vibrational energies below 7000 cm^{-1} to better than 0.05 cm^{-1} and the thermally averaged values of HFCC at a temperature $T = 300$ K to better than 0.002%.

The rovibrational basis functions are generated as products of vibrational basis functions and symmetric-top rotational eigenfunctions and the rovibrational wave functions are obtained variationally by diagonalizing the full rovibrational Hamiltonian matrix[54]. Since TROVE uses symmetry-adapted basis functions, and the total-angular-momentum quantum number J is a good quantum number, the diagonalization of the Hamiltonian matrix for each irreducible representation of the $\boldsymbol{D}_{3h}$ symmetry group, and each value of J, is done separately. Another important consequence of molecular symmetry is that the nuclear spin statistical factors[59] for the $\tilde{X}\ ^2A_2''$ electronic state of CH_3 are zero for the irreducible representations A_2' and A_2'', besides for each of the doubly degenerate representations E' and E''

only one degenerate component need be treated, thus reducing the total computational expenses for CH_3 by a factor of two. For CD_3, all statistical weight factors are non-zero thus only the second argument is viable.

3.2.3 Hyperfine Coupling Constant Expectation Values

The vibrational and rovibrational expectation values of the HFCC were computed for $^{13}CH_3$ and $^{13}CD_3$ using the *ab initio* calculated coupling constant surface and the TROVE wave functions. The thermal average values for different temperatures were computed by summing over all rovibrational states the expectation values multiplied with the corresponding Boltzmann and degeneracy factors. For an ensemble of molecules in thermal equilibrium at absolute temperature T, the thermal average of the isotropic HFCC, A, is given by

$$\langle A\rangle_T = \frac{1}{Q}\sum_i g_i \exp\left(-\frac{E_{\rm rv}^{(i)}}{kT}\right)\langle A\rangle_i \tag{3.7}$$

where g_i is the degeneracy of the ith state with the energy $E_{\rm rv}^{(i)}$ relative to the ground state energy, k is the Boltzmann constant, Q is the internal partition function defined as

$$Q = \sum_i g_i \exp\left(-\frac{E_{\rm rv}^{(i)}}{kT}\right) \tag{3.8}$$

and $\langle A\rangle_i$ is an expectation value of the operator $\hat{A}$ in a rovibrational state i

$$\langle \hat{A}\rangle_i = \langle \Phi_{\rm rv}^{(i)}|\hat{A}|\Phi_{\rm rv}^{(i)}\rangle. \tag{3.9}$$

The calculation of the quantities in Eqs. (3.7)–(3.9) requires the eigenvalues $E_{\rm rv}^{(i)}$ and eigenvectors $\Phi_{\rm rv}^{(i)}$ which are obtained variationally with TROVE.

The degeneracy factor is computed as $(2J+1)g_{\rm ns}$, where $g_{\rm ns}$ is the nuclear spin statistical weight taking values in D_{3h} symmetry group in order (A_1', A_2', E', A_1'', A_2'', E'') as (8, 0, 4, 8, 0, 4) for $^{13}CH_3$, and (2, 20, 16, 2, 20, 16) for $^{13}CD_3$ (Note that the symmetry of the electronic wave function is A_2''). The convergence of

the thermal averaged values of HFCC at $T = 300$ K with respect to the maximal rotational excitation, defined by $J_{\max}$, is shown on Fig. 3.2. The values are plotted relative to the ZPVC (see Table 3.4). The energy spectrum of the heavier molecule CD_3 has a higher density than that of CH_3. In addition, CD_3 has more states allowed by spin statistics. Consequently, in CD_3, more rovibrational states become populated at a given temperature and so, higher J-values must be considered in the theoretical calculations in order to obtain converged values of the thermal averages. The computed values of the partition functions used to normalize the thermally averaged values for $T = 300$ K(96 K) are 737.08(127.10) for $^{13}CH_3$, and 7519.94(1194.11) for $^{13}CD_3$.

3.3 Results

The planar equilibrium geometry of the electronic ground state, $\tilde{X}\ ^2A_2''$, of CH_3 has $\boldsymbol{D}_{3h}$ geometrical symmetry. The normal modes ν_1 and ν_2 of CH_3 have non-degenerate symmetries A_1' and A_2'', respectively, and associated principal quantum numbers v_1 and v_2. The normal modes ν_3 and ν_4 are of doubly-degenerate symmetries E' and E'', respectively, the associated quantum numbers here are $v_3^{\ell_3}$ and $v_4^{\ell_4}$. The calculated 24 lowest vibrational energy levels of $^{12}CH_3$, $^{13}CH_3$ and $^{13}CD_3$ are listed in Table 3.1 where they are compared with the results of other theoretical studies[103, 104] and experiment [18, 125–127]. Each vibrational state is assigned by the symmetry in $\boldsymbol{D}_{3h}$(M) and vibrational quantum numbers $(v_1, v_2, v_3^{\ell_3}, v_4^{\ell_4})$ obtained from the basis function with the largest contribution to the vibrational eigenfunction. The agreement with experiment is generally good, the standard deviation for six states is 3.2 cm^{-1} which is a little improvement over the previous theoretical results of 4.6 cm^{-1} (Ref. [103]) and 7.4 cm^{-1} (Ref. [104]). The complete list of computed vibrational energies up to 8000 cm^{-1} for three isotopologues can be found in the supplementary material[120].

The calculated expectation values of the HFCC for $^{13}CH_3$ given in Table 3.2 for a number of vibrational states show a very strong dependence on v_2, the quantum number of the out-of-plane vibration. This is due to both the nonrigid character of the out-of-plane motion and the strong dependence of the coupling constant on the out-of-plane coordinate (see Fig. 3.1). Even though we need only consider one minimum of the PES here so that no tunneling motion takes place, the accurate treatment of the nonrigid character of the out-of-plane vibrational mode is very

important. This is evident from the comparison (Table 3.2) of HFCC expectation values obtained as described above with the results of a more conventional PRM approach, commonly used to compute vibrational corrections to molecular properties[67, 79]. The PRM results in Table 3.2 were obtained variationally in the present work by expanding the TROVE Hamiltonian in normal coordinates with the KEO, PES, and HFCC parts truncated after zero-, quartic- and second-order terms, respectively. All expectation values in Table 3.2 were obtained variationally but it is obvious that the use of normal coordinates and the restrictive truncation of the various series expansions introduce substantial changes in the expectation values. The PRM results deviate most from those of the nonrigid-model TROVE calculation for excited states of the out-of-plane bending mode. For such states, the deviations reach values around 10 G or 10-20%.

A 'true' PRM calculation, using perturbation theory to solve the rovibrational Schrödinger equation, would introduce additional approximations and we surmise it would produce results deviating even more from the nonrigid-model values. A complete list of HFCC vibrational expectation values for $^{13}CH_3$ and $^{13}CD_3$ is given in the supplementary material[120].

In Table 3.3, we give the theoretical equilibrium-geometry value of the HFCC for $^{13}CH_3$, the ZPVC, and the value resulting from the thermal averaging at $T =$ 96 K. These values are compared with the results of the previous theoretical studies and experiment. In the previous theoretical studies, different electronic structure methods and basis sets were used to compute the potential and coupling constant surfaces, the vibrational corrections were treated by means of perturbation theory. As can be seen from the table the HFCC value is strongly dependent on the ZPVC, which in this work is found to constitutes about 44% of the equilibrium value. The temperature correction originating in excited rotation-vibration states (i.e., the correction obtained on top of ZPVC) at $T = 96$ K is 0.02 G and thus tiny; it obviously increases with increasing temperature and attains a value of 1.0 G (see Table 3.4) for $T = 300$ K. For $^{13}CD_3$ the ZPVC is approximately 25% of the equilibrium HFCC value (25.8 G); the additional $T = 300$ K temperature correction has a small value of 1.7G.

3.4 Discussion and Summary

Table 3.3 confirms that for the theoretical, thermally averaged values of the HFCC of $^{13}CH_3$, the differences between the value at equilibrium $A_{iso}^{(eq)}$ and the vibrationally/thermally averaged value $A_{iso}^{(tot)}$ are dramatic. As mentioned previously, these differences are solely due to the effect of the ZPVC. Analysis of the contributions from the individual vibrational modes has shown that the dominant vibrational effect originates from the out-of-plane bending mode (corresponding to the 'umbrella-flipping' inversion of ammonia NH_3). Other vibrational modes contribute only slightly since the associated fundamental and overtone states are hardly populated at $T = 96$ K. In Fig. 3.1 we show the dependence of the HFCC in $^{13}CH_3$ on the out-of-plane vibrational coordinate ρ, which is defined as the angle between the three-fold rotational axis and any one of the three C–H bonds. Clearly, the strong dependence of the HFCC on ρ along with the effect of delocalization of the out-of-plane vibrational wave functions, due to the large amplitude character of the vibration, makes the corresponding expectation value and thus the contribution to the ZPVC quite substantial.

Our CCSD(T) equilibrium value $A_{iso}^{(eq)}$ agrees well with the results of previous QCISD(T) [106] and MCSCF [107] calculations (Table 3.3), with slightly larger deviation from the B3LYP result,[79] which is known to overestimate the spin polarization effect[128]. The deviations can also be partly attributed to the effect of the different basis sets used in electronic structure calculations. We employed the basis set aug-cc-pVTZ-J, specifically designed for core properties. In several studies [111, 129, 130] this basis set has proved to yield coupling constants in good agreement with experiment.

We conclude that with the high-level electronic structure method and comprehensive variational treatment of the rovibrational motion employed in the present work, we were able to obtain reliable values of the HFCC for $^{13}CH_3$ and $^{13}CD_3$ in very good agreement with experiment (Table 3.3). In particular, we calculate realistically the large vibrational contribution to the HFCC, which we found to be 44% of the equilibrium value.

In agreement with previous studies, the large vibrational contribution can be attributed to the large amplitude out-of-plane bending motion. For the temperatures considered in this study ($T < 300$ K) the thermal effects play a minor role.

TABLE 3.1: Calculated and experimental vibrational energies (in cm^{-1}) for $^{12}CH_3$, $^{13}CH_3$, and $^{13}CD_3$.

v_1 v_2 $v_3^{\ell_3}$ $v_4^{\ell_4}$	Γ[‡]	$^{12}CH_3$				$^{13}CH_3$	$^{13}CD_3$
		Present work	Ref. [103].[§]	Ref. [104].[¶]	Experiment[‖]	Present work	Present work
$0\ 0\ 0^0\ 0^0$[**]	A_1'	[6466.9]	[6449.2]	[6445.9]	–	[6446.4]	[4742.1]
$0\ 1\ 0^0\ 0^0$	A_2''	601.1	596.3	591.7	606.5	596.1	447.4
$0\ 2\ 0^0\ 0^0$	A_1'	1278.3	1278.9	1266.2	1288.1	1267.7	944.6
$0\ 0\ 0^0\ 1^1$	E'	1389	1387.5	1388.4	1397	1384.1	1022.8
$0\ 1\ 0^0\ 1^1$	E''	2001.8	1997	1991.8	–	1992.1	1475.7
$0\ 3\ 0^0\ 0^0$	A_2''	2006	2025.6	1994.2	2019.2	1989.2	1476.4
$0\ 2\ 0^0\ 1^1$	E'	2688.8	2690	2674	–	2673.7	1977.6
$0\ 0\ 0^0\ 2^0$	A_1'	2752.4	2748.2	2750.7	–	2742.4	2022.6
$0\ 0\ 0^0\ 2^2$	E'	2770.9	2766.1	2767.8	–	2761.1	2039.5
$0\ 4\ 0^0\ 0^0$	A_1'	2771.8	2829	2763.2	–	2749.6	2034.9
$1\ 0\ 0^0\ 0^0$	A_1'	3003.4	2991.5	2988.5	3004.4	3002.6	2154.1
$0\ 0\ 1^1\ 0^0$	E'	3159.5	3144.6	3142.6	3160.8	3147.3	2362.0
$0\ 1\ 0^0\ 2^0$	A_2''	3378.6	3371.1	3367.1	–	3365.0	2482.5
$0\ 1\ 0^0\ 2^2$	E''	3395.2	3388.5	3382.9	–	3380.7	2498.3
$0\ 3\ 0^0\ 1^1$	E''	3426.6	3447	3407.5	–	3405.5	2514.0
$1\ 1\ 0^0\ 0^0$	A_2''	3595.1	3575.5	3572.8	–	3587.5	2595.2
$0\ 5\ 0^0\ 0^0$	A_2''	3564.5	3686	3557.7	–	3536.3	2616.8
$0\ 1\ 1^1\ 0^0$	E''	3736.2	3716	3710.2	–	3719.5	2793.7
$0\ 2\ 0^0\ 2^0$	A_1'	4075.1	–	4057.5	–	4056.1	2989.4
$0\ 2\ 0^0\ 2^2$	E'	4091.8	–	4073.1	–	4072.1	3005.2
$0\ 0\ 0^0\ 3^1$	E'	4128.4	–	4107.7	–	4114.7	3026.1
$0\ 0\ 0^0\ 3^3$	A_1'	4144.9	–	4138.9	–	4140.4	3053.9
$0\ 0\ 0^0\ 3^3$	A_2'	4150.1	–	4138	–	4135.4	3052.4
$0\ 4\ 0^0\ 1^1$	E'	4200.2	–	4179.7	–	4172.7	3076.2
$1\ 2\ 0^0\ 0^0$	A_1'	4258.4	–	4234.3	–	4246.0	3091.2

TABLE 3.2: Vibrational energies, $E_{\rm vib}$, (in $\rm cm^{-1}$) and expectation values of HFCC (in G) computed for $^{13}CH_3$ using the TROVE variational and the perturbed-rigid-molecule (PRM) approaches (see text).

$v_1\ v_2\ v_3^{l_3}\ v_4^{l_4}$	$\Gamma^{\dagger\dagger}$	$E_{\rm vib}$	HFCC	
			TROVE	PRM
$0\ 0\ 0^0\ 0^0$	A_1'	0.0	37.1	37.6
$0\ 1\ 0^0\ 0^0$	A_2''	596.2	52.8	55.8
$0\ 2\ 0^0\ 0^0$	A_1'	1267.7	64.5	70.5
$0\ 0\ 0^0\ 1^1$	E'	1384.1	39.4	38.6
$0\ 3\ 0^0\ 0^0$	A_2''	1989.2	74.6	83.1
$0\ 1\ 0^0\ 1^1$	E''	1992.2	54.6	57.0
$0\ 2\ 0^0\ 1^1$	E'	2673.7	66.0	71.6
$0\ 0\ 0^0\ 2^0$	A_1'	2742.4	52.2	40.2
$0\ 4\ 0^0\ 0^0$	A_1'	2749.6	76.0	93.9
$0\ 0\ 0^0\ 2^2$	E'	2761.1	42.9	39.6
$1\ 0\ 0^0\ 0^0$	A_1'	3002.6	39.0	39.3
$0\ 0\ 1^1\ 0^0$	E'	3147.3	38.5	39.6
$0\ 1\ 0^0\ 2^0$	A_2''	3364.9	58.7	58.2
$0\ 1\ 0^0\ 2^2$	E''	3380.7	57.6	67.7
$0\ 3\ 0^0\ 1^1$	E''	3405.5	75.5	73.9
$0\ 5\ 0^0\ 0^0$	A_2''	3536.3	90.5	101.5
$1\ 0\ 0^0\ 0^1$	A_2''	3587.5	55.9	58.2
$0\ 0\ 1^1\ 0^1$	E''	3719.5	54.6	58.5
$0\ 2\ 0^0\ 2^0$	A_1'	4056.1	68.9	72.3
$0\ 2\ 0^0\ 2^2$	E'	4072.1	67.7	72.3
$0\ 0\ 0^0\ 3^1$	E'	4114.7	51.7	41.6
$0\ 0\ 0^0\ 3^3$	A_2'	4135.4	44.7	40.6
$0\ 0\ 0^0\ 3^3$	A_1'	4140.9	49.9	40.6
$0\ 4\ 0^0\ 1^1$	E'	4172.7	84.5	93.1
$1\ 2\ 0^0\ 0^0$	A_1'	4246.0	67.2	86.2
$0\ 6\ 0^0\ 0^0$	A_1'	4353.7	98.5	94.9
$0\ 2\ 1^1\ 0^0$	E'	4371.5	66.3	72.4
$1\ 0\ 0^0\ 1^1$	E'	4385.0	42.3	40.3
$0\ 0\ 1^1\ 1^1$	A_2'	4510.3	40.6	40.5
$0\ 0\ 1^1\ 1^1$	E'	4518.1	40.9	40.3
$0\ 0\ 1^1\ 1^1$	A_1'	4526.4	41.6	40.6
$0\ 1\ 0^0\ 3^1$	E''	4742.2	63.5	58.9
$0\ 1\ 0^0\ 3^3$	A_2''	4765.3	62.9	67.9
$0\ 1\ 0^0\ 3^3$	A_1''	4766.1	58.7	59.0
$0\ 3\ 0^0\ 2^0$	A_2''	4801.4	78.1	74.0
$0\ 3\ 0^0\ 2^2$	E''	4813.1	77.8	83.1
$1\ 3\ 0^0\ 0^0$	A_2''	4959.3	76.8	80.6
$0\ 5\ 0^0\ 1^1$	E''	4964.7	83.7	99.9
$1\ 1\ 0^0\ 1^1$	E''	4984.3	66.4	59.5

TABLE 3.3: The calculated and experimental HFCC (in G) of $^{13}CH_3$. The values listed are the electronic HFCC at equilibrium geometry, $A_{iso}^{(eq)}$, the total HFCC value including ZPVC ($T = 0$ K) and temperature ($T = 96$ K) correction, $A_{iso}^{(tot)}$, as well values of the ZPVC (/temperature) effects with respect to the equilibrium.

Method/Basis set	$A_{iso}^{(eq)}$	$A_{iso}^{(tot)}$	$A_{iso}^{(tot)} - A_{iso}^{(eq)}$	T(K)	Ref.
P(CI)/DZ	22.2	35.1	12.9(58%)	96	[105]
QCISD(T)/TZVP	27.8	37.7	9.9(36%)	96	[106]
MCSCF/cc-pVTZus2st	27.7	37.3	9.6(35%)	0	[107]
B3LYP/Huz-IIIsu3	29.9	42.2	12.3(41%)	0	[79]
CCSD(T)/aug-cc-pVTZ-J	25.8	37.1	11.3(44%)	0/96	This work
Experiment	27.0	38.3	–	96	[131]

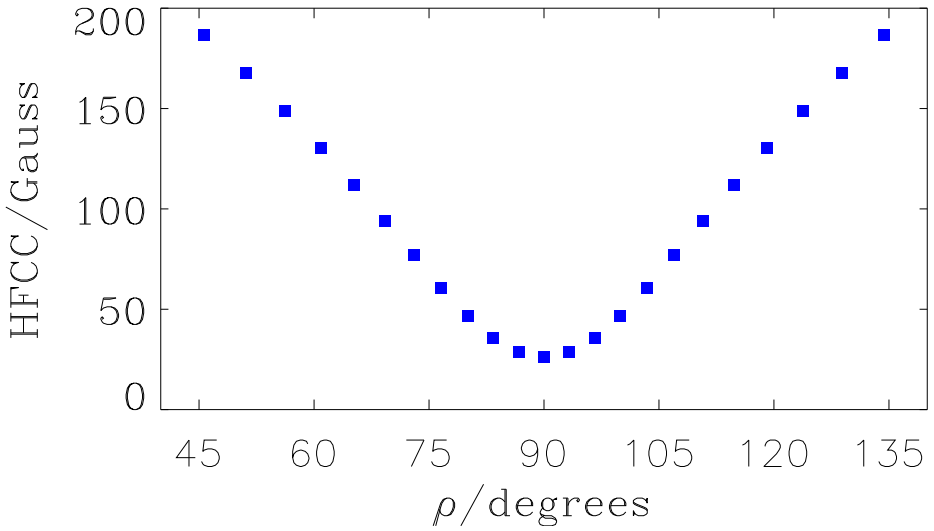

FIGURE 3.1: The HFCC in $^{13}CH_3$ calculated at the CCSD(T)/aug-cc-pVTZ-J level of theory for molecular geometries with all three C–H bond lengths fixed at 1.0759 Å and all three H-C-H bond angles equal. The HFCC is plotted as a function of ρ, the angle between the three-fold rotational axis and any one of the three C–H bonds.

TABLE 3.4: Thermal contribution to HFCC (in G) in $^{13}CH_3$ and $^{13}CD_3$.

Temp.(K)	$^{13}CH_3$	$^{13}CD_3$
0	37.068	34.239
96	37.092	34.275
300	38.076	35.917

FIGURE 3.2: Convergence of the $T = 300$ K thermally averaged HFCC vs J_{max} plotted for $^{13}CH_3$ (blue circles) and $^{13}CD_3$ (orange squares) relative to the ZPVC.

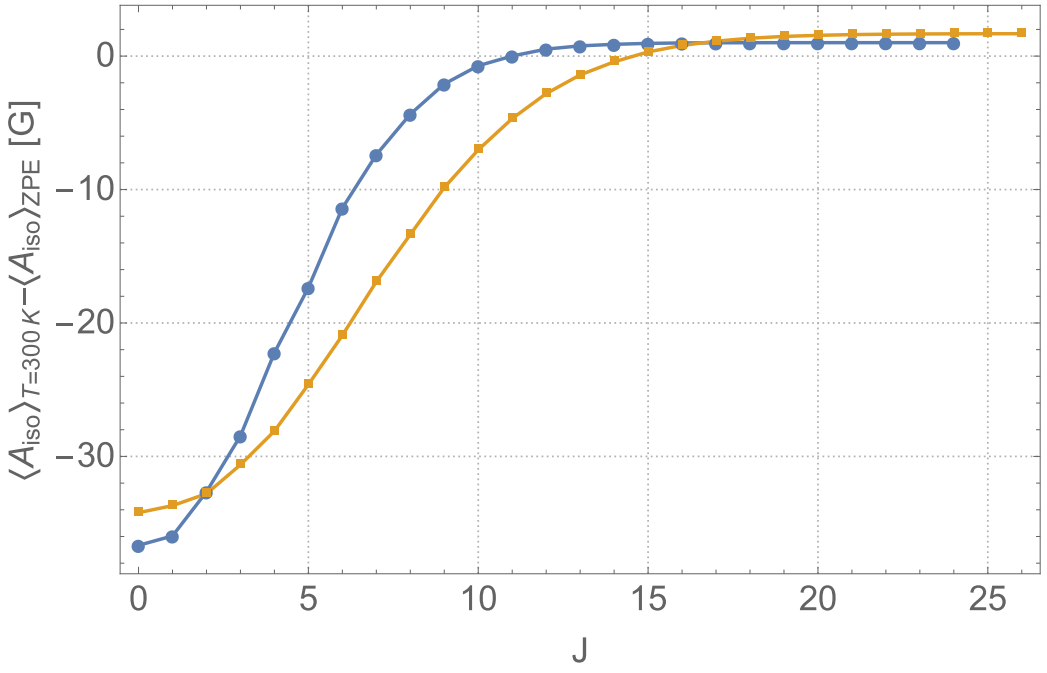

Chapter 4

Infrared Intensities

*

We present the first variational calculation of a room temperature *ab initio* line list for the CH_3 radical. It is based on a high level *ab initio* potential energy surface and dipole moment surface of CH_3 in the ground electronic state. The rovibrational energy levels and Einstein A coefficients were calculated variationally using the methods implemented in the computer program TROVE. Vibrational energies and vibrational intensities are found to be in very good agreement with the available experimental data.

4.1 Introduction

In the infrared region, CH_3 intense out-of-plane bending mode, ν_2, located at 606 cm^{-1}, provides a convenient band for concentration measurements, and this feature has been used extensively for this purpose [22, 132–134]. However, this method relies on the knowledge of the transition intensities associated with the corresponding transition dipole moment, μ_2, of the ν_2 band.

In this chapter we apply a high level *ab initio* potential energy and dipole moments surfaces to compute a room temperature line list for CH_3 using the TROVE program [53–56].

*Adapted with permission from (J. Phys. Chem. A 2019, 123, 4755). Copyright 2019 American Chemical Society.

4.2 The methyl radical quantum numbers

At equilibrium, the three protons of electronic-ground-state $\tilde{X}\ ^2A_2''$ CH_3, a symmetric top molecule, form an equilateral triangle with the C nucleus at the centre-of-mass of the planar structure with $\boldsymbol{D}_{3h}$ point group symmetry (see Table A-10 of Ref.59).

Six coordinates are required to define the internal vibrational motion of a tetratomic molecule, of which, in the case of CH_3, two are doubly degenerate. The standard Herzberg convention [135] labels the symmetric stretch and symmetric bend as v_1 and v_2 respectively, and the asymmetric stretch and asymmetric bend as v_3 and v_4 respectively. The latter two are degenerate, and as a result additional quantum numbers are required in the form of the vibrational angular momenta l_3 and l_4, respectively.

The rotation of CH_3 is specified by the total angular momentum N [†] , its projection on the body-fixed axis (molecular symmetry axis) K and the parity τ_{rot} or, alternatively the symmetry of the rovibrational states Γ in the molecular symmetry group[59] $\mathcal{D}_{3h}(M)$ to which CH_3 belongs.

The rigorous selection rules which determine the allowed electric dipole transitions of CH_3 are $\Delta N = N' - N'' = 0, \pm 1$ $(N'' + N' \geq 1)$ with symmetry selection rules $A_1' \leftrightarrow A_1''$, $A_2' \not\leftrightarrow A_2''$, and $E' \leftrightarrow E''$.

4.3 The dipole moment surface

The *ab initio* dipole moment surface (DMS) for the electronic ground state of CH_3 was computed using the MOLPRO[118] program package. Frozen-core calculations were carried out for 19 369 symmetry-unique geometries using the spin-restricted open-shell coupled cluster theory RCCSD(T) [136, 137] and the augmented correlation consistent valence basis set aug-cc-pVTZ [138, 139] employing the two-point stencil central finite differences with the electric field strength of 0.002 a.u.

The DMS was determined on a six-dimensional grid consisting of 19369 geometries with coordinates in the ranges $r_i = 0.8$ Å – 1.20 Å for bond distances and $\alpha_i = 80°$

[†]In the case of open-shell molecules, like CH_3, the total angular momentum is denoted as N exculding the non-zero eletron spin angluar momentum, S, and denoted as J with the inclusion of S.

– 120° for bond angles, where $i = 1, 2, 3$. The r_i is the instantaneous value of the internuclear distance C–H_i, and the bond angles are given as $\alpha_1 = \angle(H_2CH_3)$, $\alpha_2 = \angle(H_1CH_3)$, and $\alpha_3 = \angle(H_1CH_2)$. The DMS is finally, employing the so-called symmetrized molecular-bond representation [124], expressed analytically with a mathematical function in terms of the internal coordinates of the molecule.

4.4 The intensity simulations with TROVE

4.4.1 General formulas

The line strengths, $S(f \leftarrow i)$, for any rovibrational transition between the energy levels must satisfy the selection rules. After calculating $S(f \leftarrow i)$, Einstein coefficients and absorption intensities can be computed.

For a transition from an initial state i with rotation-vibration wavefunction $|\Phi_{\rm rv}^{(i)}\rangle$ to a final state f with rotation-vibration wavefunction $|\Phi_{\rm rv}^{(f)}\rangle$. The line strength[59, 140, 141] $S(f \leftarrow i)$ of a rovibrational transition is

$$S(f \leftarrow i) = g_{\rm ns} \sum_{M_f, M_i} \sum_{A=X,Y,Z} \left| \langle \Phi_{\rm rv}^{(f)} \, | \bar{\mu}_A | \, \Phi_{\rm rv}^{(i)} \rangle \right|^2, \tag{4.1}$$

where the nuclear spin statistical weight factor[59] is denoted as $g_{\rm ns}$ and the electronically averaged component of the molecular dipole moment along the space-fixed axis[59] $A = X$, Y, or Z is denoted as $\bar{\mu}_A$. The quantum numbers M_i (M_f) are the projections of the total angular momentum $\hat{\mathbf{N}}$ on the Z axis for the initial (final) states.

The intensity of a spectral line at temperature T is determined by

$$I(f \leftarrow i) = \frac{8\pi^3 N_A \tilde{\nu}_{if}}{(4\pi\epsilon_0)3hc} \frac{{\rm e}^{-E_i/kT}}{Q} \left[1 - \exp(-hc\tilde{\nu}_{if}/kT)\right] S(f \leftarrow i). \tag{4.2}$$

Here $\tilde{\nu}$ is the absorption wavenumber, and Eq. (4.2) refers to the transition from the state i with energy E_i to the state f with energy E_f, where $hc\tilde{\nu}_{if} = E_f - E_i$. Q is the partition function defined as $Q = \sum_j g_j \exp(-E_j/kT)$, where g_j is the total degeneracy of the state with energy E_j and the sum runs over all energy levels of

the molecule, and other symbols have their usual meanings. The total degeneracy g_j is given by $(2N+1)$ times the electron spin degeneracy $(2S+1=2)$ and times the nuclear spin degeneracy which is 4, 0, 2, 4, 0, 2 for $A_1', A_2', E', A_1'', A_2''$, and E'' symmetries respectively (see Appendix B). The ground electronic state of CH_3 is a doublet ($\tilde{X}\ ^2A_2''$) with a small splitting[96, 126] in the rovibrational energy levels due to spin-rotation interactions, around 0.01 cm^{-1}, which we therefore chose to ignore in the present work.

Yurchenko *et al.* [140] have given, in their Eq. (21), a detailed expression for the line strength of an individual rovibrational transition within an isolated electronic state of an XY_3 pyramidal molecule. Assuming that the populations of the lower (initial) states are Boltzmann-distributed, we limit the intentity calculations to transitions starting from levels below $E_i^{\max}/hc = 4\,000$ cm^{-1}. With this limitation, Boltzmann factors of $\exp(-E_i/kT) > 4\times10^{-9}$ enter into Eq. (4.2) for $T = 300$ K. Since it is safe to limit the lower-state energies to be below 4000 cm^{-1}, it is sufficient to consider rotational states with $N \leqslant 25$. We compute a line list in the wavenumber range 0–10 000 cm^{-1}; the upper energy limit (i.e., the maximum value of the final-state energy) corresponds to a term value of $E^{\max}/hc = 14{,}000$ cm^{-1}.

4.4.2 Computational details

The variational nuclear-motion calculations are done with a symmetry-adapted basis set. With such a basis set, the Hamiltonian matrix becomes block diagonal according to the irreducible representations of the $\boldsymbol{D}_{3h}(M)$ molecular symmetry group:[59] A_1', A_2', A_1'', A_2'', E', and E''. The A_2' and A_2'' matrices are of no interest for CH_3 as the corresponding states have zero nuclear spin statistical weights and do not exist in nature[59] (Appendix B).

The calculation of the matrix elements $\langle\Phi_{\rm rv}^{(f)}|\bar{\mu}_A|\Phi_{\rm rv}^{(i)}\rangle$ in Eq. (4.1) is the bottleneck in the spectrum simulations. Here, the wavefunctions $\Phi_{\rm rv}^{(w)}$ are given as superpositions of symmetry-adapted basis functions (see Eq. (65) of Yurchenko *et al.* [56]):

$$|\Phi_{\rm rv}^{(w)}\rangle = \sum_{VK\tau_{\rm rot}} C_{VK\tau_{\rm rot}}^{(w)} |N_w\, K\, m_w\, \tau_{\rm rot}\rangle\, |V\rangle, \quad w = i \ \text{ or } \ f, \tag{4.3}$$

with the $C^{(w)}_{VK\tau_{\rm rot}}$ as expansion coefficients. In Eq. (4.3), the symmetrized rotational basis functions are denoted $|N_w\, K\, m_w\, \tau_{\rm rot}\rangle$ with $\tau_{\rm rot}$ (= 0 or 1) defining the rotational parity, and $|V\rangle$ is a vibrational basis function. In order to accelerate this part of the calculation, we pre-screened the expansion coefficients $C^{(f)}_{VK\tau_{\rm rot}}$. All terms with coefficients less than the threshold value of 10^{-13} were discarded in the intensity calculation.

The evaluation of the dipole moment matrix elements $\langle\Phi^{(f)}_{\rm rv}|\bar{\mu}_A|\Phi^{(i)}_{\rm rv}\rangle$ has been made more efficient in a two-step procedure. In the first step, an effective line strength is evaluated for a given lower state i:

$$S^A_{i,VK} = \langle\Phi^{(i)}_{\rm rv}|\bar{\mu}_A|\phi_{VK}\rangle. \tag{4.4}$$

Here, ϕ_{VK} is a short-hand notation for the primitive basis function $|N_w K\, m_w\, \tau_{\rm rot}\rangle$ $\times|V\rangle$. From the $S_{i,VK}$-values obtained, we compute, in the second step, the line strength $S(f \leftarrow i)$ as

$$S(f \leftarrow i) = g_{\rm ns} \sum_{m_i,m_f} \sum_{A=X,Y,Z} \left| \sum_{V,K} C^{(f)}_{VK\tau_{\rm rot}} S^A_{i,VK} \right|^2 . \tag{4.5}$$

We had to compute a very large number of transitions satisfying the selection rule $|N_f - N_i| \leqslant 1$, where N_i and N_f are the values of the angular momentum quantum number N for the initial and final state, respectively. Consequently, we saved memory by organizing the calculation of the rovibrational eigenstates and the $S(f \leftarrow i)$-values such that at a given time, only eigenvectors for states with two consecutive N-values, N and $N+1$, are available for the computation of $S(f \leftarrow i)$-values [57].

4.4.3 The J=0-contraction

The vibrational basis set $|V\rangle$ is obtained in TROVE using a multi-step contraction and symmetrization procedure, starting from local primitive basis set functions, each depending on one variable only (see Refs. 54–56 and references therein). Thus, a compact representation of the vibrational basis set is obtained in a form optimized for the, non-rotating, molecule of interest assuming a zero total angular momentum ($J = N + S = 0$). The final vibrational basis set is represented by

the eigenfunctions of the purely vibrational part of the Hamiltonian; we call these eigenfunctions the '$J = 0$ basis'.

4.5 Results

4.5.1 Refinement of the potential energy surface

The potential energy surface (PES) employed for the electronic ground state of CH_3 in the present work is based on the *ab initio* surface reported in Ref.120, which we denote as PES-1 (see Chapter 3).

The analytical form of PES-1[120] is given in terms of the *ab initio* cc-pVQZ-F12 values of the equilibrium structural parameters, $r_e = 1.07736927$ Å and $\alpha_e = 120°$,[120] for the electronic ground state of CH_3. In the present work, we optimized the value of r_e in a least-squares fitting to experimentally derived to rotational energy spacings within the vibrational states of CH_3. The fitting produced $r_e = 1.0762977119$ Å; $\alpha_e = 120°$ by symmetry. We use these optimized values of the equilibrium structural parameters. All results presented below are based on the analytical potential energy function called PES-2, obtained from PES-1[120] by replacing the *ab initio* cc-pVQZ-F12 value of r_e by the adjusted value given here. The remaining PES-2 parameter values are identical to those of PES-1 and can be obtained from the supplementary material to Ref. 120. The new equilibrium parameters are given in Table 4.1.

4.5.2 Basis set convergence and empirical adjustment of the vibrational band centers

The dimensions of the Hamiltonian matrix blocks to be diagonalized are important in determining the accuracy of the computed energies and wavefunctions for highly excited rovibrational states. Consequently it is imperative to determine empirically the smallest basis set with which the required eigenvalue accuracy (i.e., the optimum basis-set size for 'convergence') can be attained.

In TROVE, the size of the vibrational basis set is controlled by polyad number truncation.[53–55] For CH_3, the polyad number P is defined as:

$$P = 2(n_1 + n_2 + n_3) + n_4 + n_5 + n_6, \tag{4.6}$$

where n_i are the principal quantum numbers associated with the primitive functions $\phi_{n_i}(\xi_i)$. The primitive vibrational basis functions are products of one-dimensional basis functions $\phi_{n_i}(\xi_i)$, and only products with $P \leq P_{\max}$ are included in the primitive vibrational basis.

An even tighter level of convergence could be achieved for the vibrational term values if these were calculated with different $P_{\max}$-values and the resulting progression of term values were extrapolated to the complete vibrational basis set limit [142]. However, for the purpose of generating line lists this is not considered necessary. The corrections from the extrapolation will be small compared with the term-value errors caused by the imperfection of the underlying potential energy surface. Instead, we pragmatically aim for a higher accuracy by resorting to an empirical approach: The theoretical vibrational term values are replaced by the available accurate, experimentally derived vibrational band-centre values. In this manner, we are adjusting the vibrational band centers 'manually'; this empirical adjustment also shifts the rotational energy-level structure towards better agreement with experiment. We call this procedure the EBSC scheme as it can be regarded as an Empirical Basis Set Correction.

We adopt the EBSC scheme for the vibrational bands ν_2, $2\nu_2$, ν_1, ν_4^1, and ν_3^1, for which accurate experimental data are available, in combination with PES-2, where we have adjusted the equilibrium structure of the molecule to fit the experimentally derived pure rotational term values. The vibrational basis set was truncated at the polyad number $P_{\max} = 32$. We incorporate experimental information in the EBSC scheme, and so we obviously depart from a purely *ab initio* approach. This is considered justified by the accuracy improvement that can be achieved in the computation of an extensive rovibrational line list.

To improve the accuracy of the predicted vibrational band-centers, a more thorough refinement of the PES would be required. However, the available accurate experimental data for the vibrationally excited states of CH_3 is severely limited, and so we opted for the EBSC approach in conjunction with the r_e-refinement. For all bands that are not EBSC-corrected, the predicted vibrational term values

are determined to a significant extent by the *ab initio* data, and so their accuracy is limited. However, we have improved the prediction of the rotational structures, and that will facilitate the assignments of future experimental spectra for CH_3.

In Table 4.2, the vibrational term values below 5000 cm^{-1} of the methyl radical, calculated variationally in the present work from PES-2, are compared with the available experimental data. The EBSC substitution was made in the $N > 0$ TROVE calculations of the present work, in that the theoretical vibrational term values (obtained for $P_{max} = 32$) were replaced by the experimental values in Table 4.2. This table also shows the effect of the polyad number P_{max} on the vibrational energy.

4.5.3 Vibrational transition moments

The vibrationalnal transition moments are defined as

$$\mu_{V'V} = \sqrt{\sum_{\alpha=x,y,z} |\langle V' \mid \bar{\mu}_\alpha \mid V\rangle|^2} \tag{4.7}$$

where $|V'\rangle$ and $|V\rangle$ denote $J = 0$ vibrational wavefunctions and $\bar{\mu}_\alpha$ is the electronically-averaged dipole moment in the molecular frame. For calculation of vibrational transition moments we used our *ab initio* PES-1 and truncated the vibrational basis set at polyad number $P_{max} = 32$. A number of computed transition moments for the strongest lower lying bands are listed in Table 4.3 where they are compared with the available experimental data. The agreement with experiment is good.

From our experience, we do not believe that the 'upgrade' of the *ab initio* dipole moment surface from CCSD(T)/aug-cc-pVTZ to CCSD(T)/aug-cc-pVQZ will significantly affect the values of μ_{fi} which implies that the *ab initio* DMS is usually converged at this level. The complete list of theoretical transition moments is given as Supporting Information[143].

4.5.4 Intensity simulations

The simulation of absorption spectra at a given temperature T and within a particular wavenumber interval requires knowledge of the upper and lower-state energies

and the Einstein coefficients $A(f \leftarrow i)$ [or the line strengths $S(f \leftarrow i)$; the relationship between $A(f \leftarrow i)$ and $S(f \leftarrow i)$ is described in Ref. 140] for all transitions in the chosen wavenumber range. In practice, however, the transitions with intensities below a chosen limit are discarded. The most straightforward presentation of the spectral data is a 'stick' diagram with the stick heights representing the integrated absorption coefficients from Eq. (4.2). We report here such simulations for the CH_3 absorption bands in the wavenumber interval 600–1200 cm^{-1} for the out-of-plane bending mode ν_2. The line strengths in Eq. (4.2) are computed from Eq. (4.1) with the spin statistical weights g_{ns} from Ref. 120. The simulations are based on PES-2 and the computed DMS described above. The partition-function value used was $Q = 732.734$, obtained at 300 K as a summation over all variational term values ($N \leq 25$) below 36871.73 cm^{-1}. We have computed 22 805 378 transitions.

Figure 4.1 shows the simulated ($T = 300$ K) simulated emission spectrum (TROVE) at two different levels of theory (rovibrational and pure vibrational) and experimental spectrum of CH_3 for the 600-1200 cm^{-1}range. Our intensities based on the *ab initio* DMS are in very good qualitative agreement with experiment. This can be better appreciated in the 2000K vibrational simulation in Figure 4.1 where the first four band systems (575–625 cm^{-1}, 650–700 cm^{-1}, 725–750 cm^{-1}, and 775–800 cm^{-1}) are shown in more detail. There is no large deviation from the experimental intensities observed around 600–800 cm^{-1}.

Hermann and Leone [144] produced the methyl radical after a molecular photofragmentation process of the methyl iodide. With the dissociation of the C-I bond, they suggested that the initial energy of the CH_3 radical is concentrated in the ν_2 vibrational mode and due to the strongly repulsive nature of the dissociated molecule, the fragments will be in highly excited states. Excitation up to $\nu_2 = 10$ has observed in their emission experiment. Therefore, in order to simulate the emission spectrum at elevated temperatures with our incomplete line list a one-band model (the fundamental ν_2 band in this case) from our the parent rovibrational line list has been employed for the other hot vibrational bands of the ν_2 mode.

The procedure is as follows: after producing the 300 K cross sections using the ExoCross code [145], we filtered the ν_2 band with Gaussian profile of hwhm=8.5 cm^{-1} from 0 to 1200 cm^{-1} for 1201 points. Then we shifted the center of the ν_2 cross sections to zero (-606.453100 cm^{-1}) and normalized it. The following step

is to run a local version of ExoCross, using the vibrational transition moments to produce the vibrational band intensity at the band centers ν_{fi} together with the ν_2 band-profile, scaled by the vibrational intensity. Our results compared to the experiment is shown in Figure 4.1 on page 48. The details of the model can be found in [146].

Our complete CH_3 line list is given as Supporting Information[143].

It provides transition energies, line strengths, Einstein coefficients $A(f \leftarrow i)$ and the temperature dependent partition function $Q(T)$. We expect the line list to be applicable for temperatures below 300 K. However, the simulated spectra will become increasingly inaccurate with increasing temperature. The line list is given in the ExoMol format[147] which can be used together with the ExoCross program[145] to generate spectra of CH_3.

4.6 Conclusion

We report here simulations of spectra for the methyl radical, extending over a significant portion of the infrared spectral region. The positions and intensities calculated for the transitions are in excellent agreement with experiment, as demonstrated by detailed comparisons with observed room temperature spectra.

The CH_3 line list of the present work will facilitate detections of the methyl radical in space. In the present work we have generated, refined, and validated the potential energy and dipole moment surfaces required for the spectral simulations, and we have established the level of accuracy attainable in variational nuclear-motion calculations with our computational resources. We have produced a methyl radical line list consisting of 22.8 million transitions between 3,671,465 energy levels for rovibrational states up to $N_{\max} = 25$ and energies up to 20 000 cm^{-1}.

TABLE 4.1: Theoretical Rotational Term Values ($N \leq 5$, in cm^{-1}) of CH_3 Computed with TROVE Using Different Equilibrium Structure Parameters.

States			Term values cm^{-1}		
N	K	τ_{rot}	Obs.	Obs.-I[a]	Obs.-II[b]
1	1	0	14.3189	0.032377	0.004027
2	0	1	57.4396	0.112005	-0.002023
2	2	0	38.1186	0.092340	0.017004
2	1	0	52.6112	0.106875	0.002511
3	3	0	71.3965	0.179934	0.038989
3	2	0	95.5353	0.203902	0.014649
3	1	0	110.0032	0.219365	0.001200
4	0	0	191.2473	0.375024	-0.004034
4	4	0	114.1491	0.295456	0.070301
4	2	0	172.0038	0.353500	0.012772
4	3	0	147.9203	0.327970	0.035289

I[a] Using $r_e = 1.07736927$ Å and $\alpha_e = 120.0°$

II[a] Obtained using $r_e = 1.0762977119$ Å and $\alpha_e = 120.0°$

TABLE 4.2: Vibrational band centers (cm^{-1}) of $^{12}CH_3$ from variational calculations.

Γ	State	Ref.	Obs.[a]	$P_{max} = 24$[b]	$P_{max} = 32$[c]
A_1'	$2\nu_2$	[125]	1288.1	1279.77	1288.09
	$2\nu_4$			2737.63	2739.64
	$4\nu_2$			2773.65	2776.85
	ν_1	[18]	3004.0	3002.71	3004.41
	$2\nu_2 + 2\nu_4$			4070.04	4073.58
	$3\nu_4^3$			4118.59	4120.58
	$\nu_1 + 2\nu_2$			4258.97	4260.53
	$6\nu_2$			4391.99	4397.00
	$\nu_3^1 + \nu_4^1$			4537.94	4538.93
	$4\nu_4$			5371.39	5364.55
	$2\nu_2 + 3\nu_4^3$			5475.84	5480.07
	$4\nu_2 + 2\nu_4$			5601.91	5607.20
E'	ν_4^1	[127]	1397.0	1385.99	1387.26
	$2\nu_2 + \nu_4^1$			2688.80	2691.60
	$2\nu_4^2$			2759.77	2762.04
	ν_3^1	[126]	3160.8	3158.88	3160.82
	$3\nu_4^1$			4074.69	4075.46
	$2\nu_2 + 2\nu_4^2$			4087.92	4091.72
A_1''	$\nu_2 + 3\nu_4^3$			4767.07	4770.24
	$\nu_2 + \nu_3^1 + \nu_4^1$			5113.76	5115.37
	$3\nu_2 + 3\nu_4^3$			6235.97	6240.33
	$\nu_2 + \nu_3^1 + 2\nu_4^2$			6492.93	6494.01
	$3\nu_2 + \nu_3^1 + \nu_4^1$			6504.24	6507.12
E''	$\nu_2 + \nu_4^1$			2000.24	2002.22
	$\nu_2 + 2\nu_4^2$			3388.24	3391.11
	$3\nu_2 + \nu_4^1$			3426.45	3430.06
	$\nu_2 + \nu_3^1$			3736.40	3736.96
	$\nu_2 + 3\nu_4^1$			4726.62	4728.61
	$3\nu_2 + 2\nu_4^2$			4835.22	4839.85
	$\nu_1 + \nu_2 + \nu_4^1$			4980.92	4983.16

[a] Experimental values of band centers

[b] Computed using the $P_{max} = 24$ basis set in conjunction with the PES[120].

[c] Computed using the $P_{max} = 32$ basis set in conjunction with the PES[120].

TABLE 4.3: Band Centers ν_{fi} and Vibrational Transition Moments μ_{fi} for CH_3: Transitions originating in the vibrational ground state except for one hot band ($2\nu_2 \leftarrow \nu_2$).

States		$\nu_{fi}/\mathrm{cm}^{-1}$	calc. μ_{fi}/D	obs. μ_{fi}/D	Ref.
f	i				
$2\nu_2$	ν_2	678.81355	0.25684684	0.31(6)	[134]
ν_2	0	602.43041	0.204031249	0.215(25)	[22, 132, 133]
ν_3^1	0	3158.83077	0.039997347	0.03(27)	[148, 149]
ν_4^1	0	1387.26389	0.029311184		
$2\nu_3 + \nu_4$	0	4529.7417	0.020487697		
$\nu_1 + \nu_4^1$	0	4383.55759	0.008656491		
$2\nu_2 + \nu_3^1$	0	4396.17926	0.004860513		
$2\nu_3^2$	0	6294.76133	0.00461563		
$\nu_1 + \nu_3^1$	0	6076.67626	0.003205084		
$2\nu_4^2$	0	2762.04731	0.003133693		
$\nu_3^1 + 2\nu_4$	0	5864.94413	0.002415629		
$3\nu_4^1$	0	4075.46453	0.00185917		
$2\nu_2 + \nu_3^1 + \nu_4^1$	0	5789.15677	0.001301802		
$4\nu_2$	0	5856.38651	0.00116353		

FIGURE 4.1: CH_3 (ν_2) simulated (top and bottom) and experimental (middle) emission spectrum

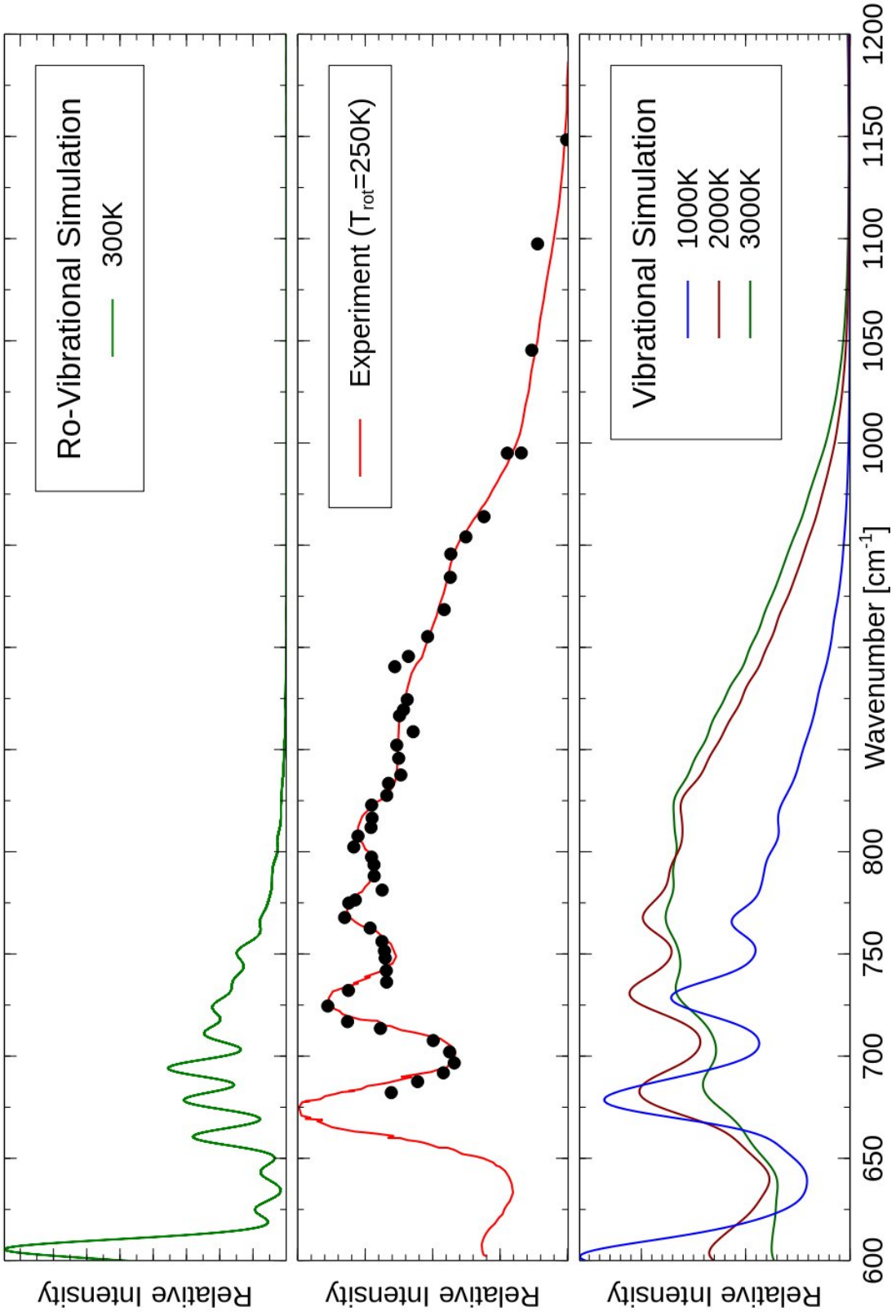

Chapter 5

Raman Intensities

Infrared absorption/emission spectroscopy (IR) is an essential tool for detecting rovibrational transitions. However, there are many transitions which cannot be observed with this technique. Not because of their weak transition intensities and the requirements of special techniques but fundamentally due to selection rules. Raman spectroscopy represents a complementary tool to IR absorption/emission spectroscopy techniques. Some rovibrational and fundamental vibrational transitions can only be detected with Raman spectroscopy. For the methyl radical, the ν_1 fundamental band can only be observed by Raman spectroscopy as well as two other fundamental bands, ν_3 and ν_4. While the most intense band, ν_2, can only be observed with infrared absorption/emission spectroscopy and it is reported in chapter 4. In this report, we successfully simulated the Raman spectrum of the ν_1 fundamental band the methyl radical as well as the $2\nu_2$ band. We conclude that with our variational treatment we are able to predict accurately Raman transitions in the electronic ground state of CH_3 in agreement with the available experimental data[150].

5.1 Introduction

The field of high-resolution infrared (IR) spectroscopy is important in many branches in science. Modeling high-resolution spectra with advanced theoretical and computational techniques is certainly a powerful tool to this field. Theoretical prediction of the rovibrational absorption spectra of many small molecules has a long history and now it is well developed [40]. Calculations for IR intensities are implemented in

many software packages [151]. IR absorption/emission spectroscopy is an essential tool for detecting rovibrational transitions. However, there are many transitions which cannot be observed with this technique. Not because of their weak transition lines and the requirements of special techniques but fundamentally due to selection rules.

Another, complementary technique to IR spectroscopy is the Raman scattering of light. In other words, Raman spectroscopy can provide information that can not be extracted from IR spectroscopy. Moreover, it is now a tool for planetary exploration[152, 153]. For the methyl radical, the ν_1 fundamental band can only be observed by Raman spectroscopy as well as two another fundamental bands, ν_3 and ν_4.

Modeling high-resolution Raman spectrum is still missing and is not well developed like IR. Theoretical attempts to model Raman spectrum (computed energies and intensities) with electronic structure methods started in the 1980s for closed-shell self-consistent field (SCF) wave functions [154–156]. To include electron correlation effects to SCF wave functions, DFT [157–159] methods and post-Hartree-Fock methods [160–163] have been developed. Relativistic effects are also important in some cases and have been applied to some diatomic [164] and triatomic molecules [165] with heavy atoms using the Dirac-Hartree-Fock method.

The development of electronic structure methods for computing Raman intensities is still an active area of research for example: studying new systems like crystalline materials [166], investigating new phenomena like hyper-Raman [167], and application to surface-enhanced Raman Scattering [168].

Theoretical study of the Raman effect will include computations of the molecular polarizability tensor. However, if the study extended to include the magnetic dipole and electric quadrupole tensors we would be able to investigate the optical activity phenomena, namely the Raman Optical activity (ROA) [169]. The conventional electronic optical activity is limited to molecules with chromophores. On the other hand, vibrational Raman optical activity (VOA) could be applied to chiral molecules which lack a chromophore. A drawback of VOA is that optical activity will be proportional to the frequency of infrared region which is smaller in magnitude compared to the UV region. Raman optical activity can overcome this weakness in VOA because we can use visible and UV light to obtain the Raman spectrum.

Electronic structure methods have been developed to deal with ROA [170, 171]. There is a recent observation also of paramagnetic ROA in which the ROA is measured in the presence of static magnetic field [172] to enhance the Raman signal. The ability of surface-enhanced Raman scattering (SERS) to enhance Raman intensities encourage researchers to extend this technique to ROA [173–175].

The weak intensity of Raman spectroscopy can be greatly enhanced with the resonance Raman technique[176–179]. In a recent study[180], shows that some terms from the theory of resonance Raman could also be important to nonresonant cases.

Most of electronic structure methods are based on the double-harmonic approximation. The expansion of the potential energy function with respect to the vibrational coordinates (rotational motions are ignored here) is truncated after the quadratic term. The second approximation arise when we take into account only the linear term in the expansion of the porlarizability tensor components. To model high-resolution Raman spectra this assumption is no longer valid for high accuracy calculations.

In this paper we apply a high level *ab initio* potential energy and polarizability surfaces to compute Raman transitions for CH_3 using the TROVE [54, 55] program.

5.2 Theory and Computational Details

To compute the Raman transition variationally, we need first to compute the multidimensional surfaces for the electronic energies and the electronic polarizability surface of CH_3.

5.2.1 Ab initio calculations

The ab initio energies required for constructing the PES for the electronic ground state of CH_3 were calculated with the MOLPRO program package. Frozen-core calculations were carried out for 24000 symmetry-unique geometries at the ROHF-RCCSD(T)/aug-cc-pVTZ level of theory.

5.2.2 Raman transitions

When linearly polarized incident radiation interacts with a molecule, radiation will be scattered in all directions. For a freely orientable molecules in a sample, this can described in terms of the average of the transition matrix elements of the polarizability tensor expressed as the Cartesian components of the laboratory fixed axis system. We discuss here the rovibrational Raman transitions within the electronic ground state. The Raman intensity for a molecule in the gas phase at thermal equilibrium can be expressed as the differential scattering cross section

$$\left[\frac{d\sigma_k}{d\Omega}(\nu_0)\right]_{\text{Stokes}} = \left(\frac{\pi}{\epsilon_0}\right)^2 \times (\nu_0 - \nu_k)^4 \times \frac{\exp(-E_i/kT)}{Z_v} \times \sum_{FF'} |\langle \Phi'_{rv}|\alpha_{FF'}|\Phi''_{rv}\rangle|^2 \tag{5.1}$$

Here F (F = X,Y,Z) is the F-coordinate of the laboratory fixed frame, ϵ_0 is the vacuum permittivity, ν_0 is the wavenumber of the incident laser beam, ν_k is the wavenumber of the incident laser beam (A laser source is needed to observe the weak, by nature, Raman intensity), Z_v is the vibrational partition function, $\langle \Phi'_{rv}|\alpha_{FF'}|\Phi''_{rv}\rangle$ is a transition matrix element of the polarizability tensor, T is the absolute temperature, E_i is the energy of the initial state, k is the Boltzmann constant, and Ω is the solid angle.

For the most important case when the angle between the incident and scattered radiations is 90°, it turns out that for a symmetric transition polarizability tensor and under the following experimental conditions:

(1) X-axis of the laboratory fixed frame (X, Y, Z) is the laser beam direction.
(2) Y-axis of the laboratory fixed frame (X, Y, Z) is the laser beam polarization.
(3) No analyzer and both components, X and Y, are considered for the Raman signal polarization.

The differential Raman scattering cross section for a rovibrational transition is then

$$\left[\frac{d\sigma_k}{d\Omega}(\nu_0)\right]_{Stokes} = \left(\frac{\pi}{\epsilon_0}\right)^2 \times (\nu_0 - \nu_k)^4 \times \frac{\exp(-E_i/kT)}{Z_v} \times |\langle \Phi'_{rv}|\alpha_{YY}|\Phi''_{rv}\rangle|^2 + |\langle \Phi'_{rv}|\alpha_{YX}|\Phi''_{rv}\rangle|^2 \tag{5.2}$$

For the efficient evaluation of transition polarizability tensor components, $\langle \Phi'_{rv}|\alpha_{\rho\sigma}|\Phi''_{rv}\rangle$, we apply the transformation properties under rotation of the irreducible transition polarizability tensor components. The irreducible tensor components are related to the Cartesian components $(\rho, \sigma = X, Y, Z)$ by

$$\alpha_{\rho\sigma} = \sum_{jm} A_{\rho\sigma,jm}\alpha^{(j)}_m \tag{5.3}$$

where $A_{\rho\sigma,jm}$ is the unitary transformation matrix

For rovibrational transitions, the matrix elements of the the irreducible transition polarizability tensor, in terms of the rovibrational basis function $|JKM, v\rangle$, are given as

$$\langle \alpha^{(j)}_m\rangle = \langle J'K'M', v'|\alpha^{(j)}_m|J''K''M'', v''\rangle \tag{5.4}$$

to relate the space-fixed irreducible tensor components $\alpha^{(j)}_m$ to their molecule-fixed components $\alpha^{(j)}_{m'}$, we use the angular momentum transformation matrices $D^{(j)}_{m',m}(\theta, \phi, \chi)$ (where (θ, ϕ, χ) are the standard Euler angles [59])

$$\alpha^{(j)}_m = \sum_{m'} \alpha^{(j)}_{m'} D^{(j)}_{m',m}(\theta, \phi, \chi) \tag{5.5}$$

Now equation 5.4 can be separated into independent rotational and vibrational parts

$$\langle \alpha^{(j)}_m\rangle = \sum_{m'=-j}^{m'=j} \langle J'K'M'|D^{(j)}_{m',m}(\theta, \phi, \chi)|J''K''M''\rangle \langle v'|\alpha^{(j)}_{m'}|v''\rangle \tag{5.6}$$

For a symmetric top molecule the value of a rotational matrix element using Winger 3-j symbol [181] is

$$\langle J^{'}K^{'}M^{'}|D^{(j)}_{m^{'},m}(\theta,\phi,\chi)|J^{''}K^{''}M^{''}\rangle = [2J^{'}+1][2J^{''}+1]\begin{pmatrix} J^{''} & j & J^{'} \\ -M^{''} & m^{'} & M^{'}\end{pmatrix}\begin{pmatrix} J^{''} & j & J^{'} \\ -K^{''} & m & K^{'}\end{pmatrix} \tag{5.7}$$

Computing rovibrational intensities for Raman Scattering are treated now by the so-called Placzek invariants [182] G_{fi}

$$(G_{fi}) = \sum_{j}(G^{(j)})_{fi} = |(\alpha^{(j)}_{m})_{fi}|^2 \tag{5.8}$$

in which

$$(G^{(j)})_{fi} = [2J^{'}+1][2J^{''}+1]\sum_{m=-j}^{m=j}\begin{pmatrix} J^{''} & j & J^{'} \\ -M^{''} & m & M^{'}\end{pmatrix}^2\sum_{m^{'}=-j}^{m^{'}=j}\begin{pmatrix} J^{''} & j & J^{'} \\ -K^{''} & m^{'} & K^{'}\end{pmatrix}^2\langle v|\alpha^{(j)}_{m^{'}}|v\rangle^2 \tag{5.9}$$

The irreducible tensor components $\alpha^{(j)}_{m^{'}}$ are given by

$$\alpha^{(0)}_{0} = -\frac{1}{\sqrt{3}}[\alpha_{xx}+\alpha_{yy}+\alpha_{zz}] \tag{5.10}$$

$$\alpha^{(2)}_{2} = \frac{1}{2}[(\alpha_{xx}-\alpha_{yy})+i(\alpha_{xy}+\alpha_{yx})] \tag{5.11}$$

$$\alpha^{(2)}_{1} = -\frac{1}{2}[(\alpha_{xz}+\alpha_{zx})+i(\alpha_{yz}+\alpha_{zy})] \tag{5.12}$$

$$\alpha^{(2)}_{0} = \frac{1}{\sqrt{6}}[2\alpha_{zz}-\alpha_{xx}-\alpha_{yy}] \tag{5.13}$$

$$\alpha^{(2)}_{-1} = \frac{1}{2}[(\alpha_{xz}+\alpha_{zx})-i(\alpha_{yz}+\alpha_{zy})] \tag{5.14}$$

$$\alpha^{(2)}_{-2} = \frac{1}{2}[(\alpha_{xx}-\alpha_{yy})-i(\alpha_{xy}+\alpha_{yx})] \tag{5.15}$$

To relate the isotropic averages of the quadratic products of the components of the Cartesian polarizability tensor in terms of Placzek rotational invariants, we have

$$\langle|\alpha_{\rho\sigma}\alpha_{\rho'\sigma'}|\rangle = \sum_{jm} A_{\rho\sigma,jm}A^{*}_{\rho'\sigma',jm}\alpha^{(j)}_{m}\alpha^{(j)*}_{m} \tag{5.16}$$

where

$$\langle|\alpha_{\rho\sigma}\alpha_{\rho'\sigma'}|\rangle = \sum_{jm} A^{(j)}_{\rho\sigma,\rho'\sigma'}G^{(j)} \tag{5.17}$$

and

$$A^{(j)}_{\rho\sigma,\rho'\sigma'} = \frac{1}{2j+1}\sum_{m}|A_{\rho\sigma,jm}A^{*}_{\rho'\sigma',jm}| \tag{5.18}$$

Therefore

$$\langle|\alpha_{xx}|\rangle^2 = \frac{1}{3}G^{(0)} + \frac{2}{15}G^{(2)} \tag{5.19}$$

and

$$\langle|\alpha_{xy}|\rangle^2 = \frac{1}{10}G^{(2)} \tag{5.20}$$

Then a general equation for a symmetric Raman scattering we will have the differential cross section in terms of Placzek invariants as

$$\begin{aligned}\left[\frac{d\sigma_k}{d\Omega}(\nu_0)\right]_{Stokes} = \left(\frac{\pi}{\epsilon_0}\right)^2 \times (\nu_0-\nu_k)^4 \times \frac{\exp(-E_i/kT)}{Z_v} \\ \times\frac{1}{30}(10G^{(0)}+7G^{(2)})\end{aligned} \tag{5.21}$$

5.3 Results

The methyl radical has four fundamental modes: the symmetric stretch, $\nu_1(A_1^{'})$, the out-of-plane bending, $\nu_2(A_2^{''})$, the degenerate asymmetric stretch, $\nu_3(E^{'})$, and the degenerate in-plane bending, $\nu_4(E^{'})$, modes. Vibrational modes with $A_1^{'}$ symmetry are only Raman active and have no infrared activity. While vibrational modes with E′ symmetry are both IR and Raman active. We study here the symmetric C-H stretch mode, $\nu_1(A_1^{'})$, of CH_3 in the electronic ground state. The experimental value of the ν_1 vibrational term value has been reported before from resonance Raman spectroscopy[16] at 3002.4 cm^{-1} and from coherent anti-Stokes Raman (CARS) spectroscopy[15] at 3004.8 cm^{-1} and at 3004.4 cm^{-1} in another CARS study[17]. Further CARS studies[18, 19] have produced similar values. With force field analysis an estimation of 3044 cm^{-1} has been reported[183] and with anharmonic correction calculations[96] a value of 2992.6 cm^{-1} was obtained. Several calculations for ν_1 have been reported with ab initio methods[97, 98, 102, 184] and with vibrational methods[103, 104]. The best prediction was 3002.0 cm^{-1} with a vibrational many-body method, the vibrational configuration interaction (VCI) method[102]. Our computational work produced [143] 3004.4 cm^{-1}.

To simulate the Raman spectrum for the methyl radical, we have computed the Placzek rotational invariants for a symmetric transition of the polarizability tensor. Equation 5.21 is then used to produce the spectrum of CH_3 in the wavenumber range from 0 to 6000 cm^{-1}. This is shown in Figure 5.1. Comparing the simulated spectrum to a one obtained from a nonresonant Raman experiment is not currently possible because no such spectrum is available in the literature, as we know. However, a resonance Raman spectrum of CH_3 has been published [16]. The difference between nonresonant Raman spectra and their resonant counterparts is that in the case of resonance, the incident laser radiation energy on our sample corresponds to that of the electronic transition. In this case of resonance the intensities of the Raman vibrational bands are greatly enhanced. Another advantage of resonance experiments is that it is possible to select to enhance a particular vibrational mode of the molecule.

Comparing our simulated Raman spectrum (Figure 5.1) to the published resonance Raman spectrum [16] may not seem completely fair. In spite of this difference between the simulated and experimental spectra, we were able to simulate some

of the Raman active modes in CH_3. The fundamental vibrational mode ν_1 at 3004.4 cm^{-1} is clearly shown. The out-of-plane fundamental mode, ν_2, of CH_3 is IR active only but the first overtone of this mode is Raman active. We are able to predict this overtone mode at 1288.09 cm^{-1}. The two modes, ν_1 and $2\nu_2$, showed rotational structure.

"The two fundamental modes ν_3 (at 3160.8 cm^{-1}) and ν_4 (at 1397.0 cm^{-1}) are Raman active but they are not assigned in the resonance Raman experiment. However, around both wavenumber values there is weak, but visible rotational structure in the experimental resonance Raman spectrum, possibly caused by these bands. Above 3160.8 cm^{-1}, the position of the ν_3 band, there are two bands noticeable in the experimental resonance Raman of Fig. 5.1, whereas three bands are present in the simulated spectrum. The two bands in the experimental spectrum are assigned as $\nu_1 + 2\nu_2$ and $2\nu_1$, respectively, while TROVE suggests the labelling $\nu_2 + \nu_3$, $4\nu_4$, and $2\nu_1$ for the three bands visible in the simulation. It is conceivable, however, that the resonance Raman technique favors other vibrational transitions than non-resonant Raman, so possibly the significant bands must be assigned differently in the two spectra."[150]

As mentioned before, CH_3 belongs to the D_{3h}(M) molecular symmetry group and therefore the fundamental ν_1 band was not observed in the several IR studies on the methyl radical. This IR inactive mode is still important to be observed; for example, in the studies on the energy distribution in methyl halide photodissociation dynamics. The solution to this problem came from Raman scattering studies and despite the weak intensity of Raman bands the ν_1 band was successfully observed. Based on the theory of rotation and vibration of molecules, in this chapter we were able successfully to predict computationally the position and intensity of the Raman active ν_1 fundamental band.

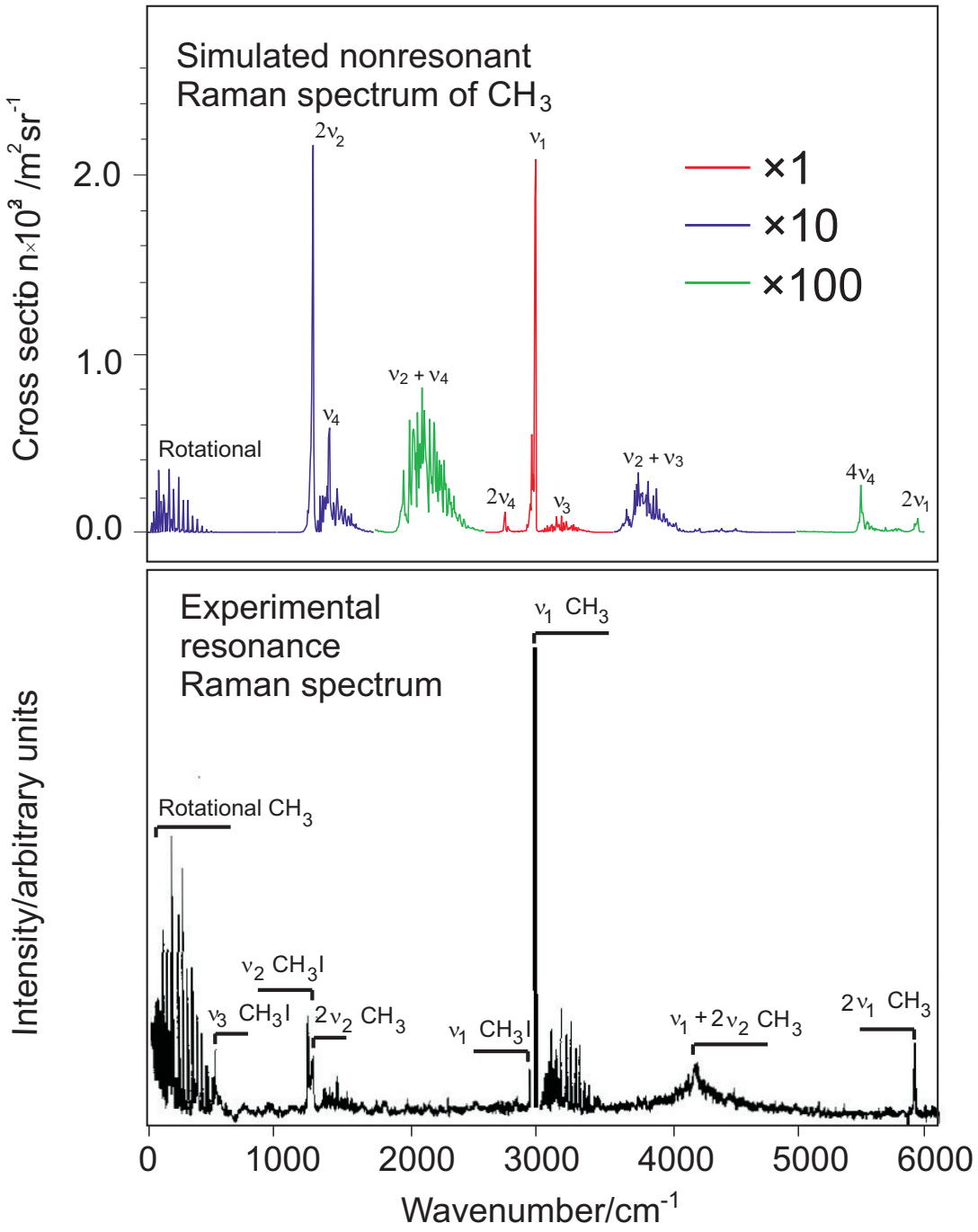

FIGURE 5.1: A comparison between Theory and Experiment for the Raman spectrum of CH_3. (Reproduced from Fig 1 of Ref. 150)

Chapter 6

Summary

The experimental study of free radicals started in 19th century. Due to the importance of these molecules in chemical reactions and to the chemical science in general, several spectroscopic observations of free radicals started but it was not an easy task at the beginning due to their short lifetimes.The methyl radical is one of the most important free radicals and plays a central role in combustion processes, in atmospheric chemistry, in the chemistry of semiconductor processing, in the chemical vapor deposition of diamond, and in many chemical processes of current industrial and environmental interest. It is also present in planetary atmospheres, and in the atmospheres of Saturn and Neptune. It is thought that CH_3 may be one of the most abundant free radicals in the interstellar medium.

Because of the central role of the methyl radical in this variety of situations, its structural and spectroscopic parameters have been the subject of numerous studies. A number of different spectroscopic techniques have been used to determine its absolute concentration in the gas phase, including UV/visible, infrared, and Raman spectroscopies. For certain experimental circumstances it is important to know the absolute concentration of a radical and this can only be carried out if accurate transition moments are available. Since the methyl radical has no electric-dipole-allowed rotational transitions (D_{3h} symmetry), IR spectroscopy (rovibrational transitions) has become one of the most suitable methods for its detection. Accurate transition moments cannot be easily measured for transitions between vibrationally excited levels and it is particularly important to be able to rely on theoretical calculations.

Based on the theory of the rotation and vibration of polyatomic molecules, implemented as the computer program TROVE, we have studied the vibrational energy levels and the rovibrational transitions of the methyl radical. Several computer programs are available to study the rotation-vibration spectroscopy of molecules but the main advantage of TROVE is the numerical preparation of the kinetic energy operator on-the-fly. In other words, it is a general program not limited to a particular type of molecule. Provided that the potential energy surface for the molecule under study is available as a mathematical function, it can be used as input for TROVE along with the construction of the KEO. In addition to complete the variational calculations, primitive basis sets such as harmonic oscillator and rigid-rotor wavefunctions will be used during the calculations. Matrix elements will be evaluated and the final Hamiltonian will be diagonalized. The output will be the rovibrational energies for a specific electronic state, usually but not necessarily the electronic ground state. If the electric dipole moment surface and the polarizability surface are given (as functions of the vibrational coordinates) in the input file for the TROVE calculations, the infrared and Raman intensities can be calculated.

The methyl radical has four fundamental modes: the symmetric stretch, $\nu_1(A_1^{'})$, the out-of-plane bending, $\nu_2(A_2^{''})$, the degenerate asymmetric stretch, $\nu_3(E^{'})$, and the degenerate in-plane bending, $\nu_4(E^{'})$, modes. Vibrational modes with A_1' symmetry are only Raman active and have no infrared activity. While vibrational modes with E' symmetry are both IR and Raman active. The most intense band, $\nu_2(A_2^{''})$, can only be observed with infrared absorption/emission spectroscopy. In chapter 4 the first variational calculation of a room temperature ab initio line list for the CH_3 radical is reported. It is based on a high level ab initio potential energy surface and dipole moment surface of CH_3 in the ground electronic state. The rovibrational energy levels and Einstein A coefficients were calculated variationally using the methods implemented in the computer program TROVE. Vibrational energies and vibrational intensities are found to be in very good agreement with the available experimental data.

Due to selection rules, Raman scattering spectroscopy represents a complementary tool to IR absorption/emission spectroscopy techniques. Certain fundamental vibrational transitions can only be detected with this technique. In chapter 5, we successfully simulated the Raman spectrum of the $\nu_1(A_1^{'})$ fundamental band of the methyl radical as well as the overtone $2\nu_2$ band. With our variational treatment

we are able to predict accurately Raman transitions in the electronic ground state of CH_3 in agreement with the available experimental data.

Not only rovibrational energies and intensities of polyatomic molecules can be studied with the TROVE computer program but also the role of the vibrational contribution to molecular properties can be computed and its significance in particular situations can be investigated. In chapter 3, we present the first variational calculation of the isotropic hyperfine coupling constant of the carbon-13 atom in the CH_3 radical for temperatures $T = 0$, 96, and 300 K. It is based on a calculated high level ab initio potential energy surface and hyperfine coupling constant surface of CH_3 in the ground electronic state. The rovibrational energy levels, expectation values for the coupling constant, and its temperature dependence were calculated variationally. Vibrational energies and vibrational and temperature effects for coupling constant are found to be in very good agreement with the available experimental data. We found, in agreement with previous studies, that the vibrational effects constitute about 44% of the constant's equilibrium value, originating mainly from the large amplitude out-of-plane bending motion and that the temperature effects play a minor role.

Since the development of quantum mechanics, theoretical chemistry has played a great role in the field of molecular science. The main goal is to model and predict experiments in difficult situations and also to help in interpreting experimental results. Herzberg was one of the pioneers of the application of quantum mechanics in spectroscopy and his work in this field were summarized by him in his a series of books termed "Molecular Spectra and Molecular Structure" in 1939, 1945, and 1966 respectively. A half a century after the publication of these series of books and the research in the field of theoretical molecular spectroscopy is still under development. For example, extending highly accurate rovibrational methods to larger molecules and exploring inactive infrared and Raman vibrational modes with non-linear methods.

Appendix A

How to obtain the Hyperfine Coupling Constant in MHz or Gauss from the *ab initio* spin density

To compute the electron-nucleus hyperfine coupling constant (HFCC), we do compute a first-order property which is the spin density [185]. The result will be in atomic units and it needs to be converted to MHz or Gauss as measured in experiments.

For example, the HFCC (in atomic units) for ^{13}C in the methyl radical is

$$A_{iso}^{N} = \frac{1}{3}\mu_0\mu_B\mu_N g_e g_N \langle S_Z \rangle^{-1} \rho(N) \tag{A.1}$$

where

A_{iso}^{N} is the isotropic hyperfine coupling constant
μ_0 is the vacuum permeability $= 4\pi \times 10^{-7}$ $[J \cdot s^2 \cdot c^{-2} \cdot m^{-1}]$
μ_B is the Bohr magneton $= 9.27{\times}10^{-24}$ $[J \cdot T^{-1}]$
g_e is the electronic g-factor $= 2.002$
$\langle S_Z \rangle^{-1}$ is the electron spin expectation value $=\frac{1}{2}$

for ^{13}C

μ_N is the nuclear magneton = 5.05×10^{-27} $[J \cdot T^{-1}]$
g_N is the nuclear g-factor = 1.4048

and at the its equilibrium geometry (H-C-H = 120° and C-H = 1.0759 $\mathring{A}$) at the UHF-CCSD(T)/aug-cc-pVTZ-J level of theory

$\rho(N)$ is the spin density = 0.064832 $[a_0^{-3}]$

This will give

$$A_{iso}^{^{13}C} = 72.88[MHz] = 26.01[G] \tag{A.2}$$

Appendix B

Nuclear Spin Statistics for CH_3

Upon permutation of the nuclei, $A_2^{'}$ and $A_2^{''}$ (from the D_{3h}(M) group) satisfy the following condition for the internal wavefunction, $\Phi_{int}^{^{12}CH_3}$, of the methyl radical

$P_{(23)}\ \Phi_{int}^{^{12}CH_3} = (-1)\ \Phi_{int}^{^{12}CH_3}$

We can define the Φ_{int} as a rovibronic wavefunction,Φ_{evr}, and a nuclear spin wavefunction, Φ_{ns}.

$\Phi_{int} = \Phi_{evr}\Phi_{ns}$

with the necessary condition for their symmetry representations

$\Gamma_{int} \subset \Gamma_{evr} \bigotimes \Gamma_{ns}$

TABLE B.1: CH_3 Character Table, The D_{3h}(M) group

D_{3h}(M)	E	(123)	(23)	E^*	$(123)^*$	$(23)^*$	
D_{3h}	E	$2C_3$	$3C_2$	σ_h	$2S_3$	$3\sigma_v$	
$A_1^{'}$	1	1	1	1	1	1	$\alpha_{zz}, \alpha_{xx}+\alpha_{yy}$
$A_1^{''}$	1	1	1	–1	–1	–1	Γ^*
$A_2^{'}$	1	1	–1	1	1	–1	$\hat{J}_z$
$A_2^{''}$	1	1	–1	–1	–1	1	T_z
$E^{'}$	2	–1	0	2	–1	0	(T_x, T_y),$(\alpha_{xx}-\alpha_{yy}, \alpha_{xy})$
$E^{''}$	2	–1	0	–2	1	0	$(\hat{J}_x, \hat{J}_y), (\alpha_{xz}, \alpha_{yz})$

TABLE B.2: The nuclear spin wavefunction for CH_3 under the symmetry operations of the $D_{3h}(M)$ group

Φ_{ns}	E	(123)	(23)	E^*	$(123)^*$	$(23)^*$
$\alpha\alpha\alpha$	1	1	1	1	1	1
$\alpha\alpha\beta$ $\alpha\beta\alpha$ $\beta\alpha\alpha$	3	0	1	3	0	1
$\alpha\beta\beta$ $\beta\alpha\beta$ $\beta\beta\alpha$	3	0	1	3	0	1
$\beta\beta\beta$	1	1	1	1	1	1
total	8	2	4	8	2	4

Applying the projection operator on the nuclear spin wavefunctions

$$a_i = \frac{1}{h}\sum_R \chi^{\Gamma}[R]\chi^{\Gamma_i}[R]^*$$

we obtain

$\Gamma_{ns} = 4A_1' \bigoplus 2E'$

For Γ_{ns} with A_1' (multiplicity=4) and E' (mulitplicity=2)

$\Gamma_e \otimes \Gamma_{vr} \otimes \Gamma_{ns} = \Gamma_{int}$				$\Gamma_e \otimes \Gamma_{vr} \otimes \Gamma_{ns} = \Gamma_{int}$			
A_2''	A_1'	A_1'	A_2''	A_2''	A_1'	E'	E''
A_2''	A_1''	A_1'	A_2'	A_2''	A_1''	E'	E'
A_2''	A_2'	A_1'	A_1''	A_2''	A_2'	E'	E''
A_2''	A_2''	A_1'	A_1'	A_2''	A_2''	E'	E'
A_2''	E'	A_1'	E''	A_2''	E'	E'	$A_1' \bigoplus A_2' \bigoplus E'$
A_2''	E''	A_1'	E'	A_2''	E''	E'	$A_1'' \bigoplus A_2'' \bigoplus E''$

allowed rovibrational states

zero-statistical weights

Γ_{int} must span A_2' or A_2''

Bibliography

[1] E. J. B. Willey. Free radicals in the electric discharge. *Trans. Faraday Soc.*, 30:230–245, 1934.

[2] W. D. McGrath and T. Morrow. Identification of Free Radicals in Flash Photolysis. *Nature*, 204:988–989, 1964.

[3] Alan Carrington. *Microwave Spectroscopy of Free Radicals*. Academic Press, London, 1974.

[4] Dolphus E. Milligan and Marilyn E. Jacox. Matrix-Isolation Study of the Infrared and Ultraviolet Spectra of the Free Radical NCO. *J. Chem. Phys.*, 47:5157–5168, 1967.

[5] James A. Miller, Robert J. Kee, and Charles K. Westbrook. Chemical Kinetics and Combustion Modeling. *Annu. Rev. Phys. Chem.*, 41:345–387, 1990.

[6] R. Ravishankara. Kinetics of radical reactions in the atmospheric oxidation of CH_4. *Annu. Rev. Phys. Chem.*, 39:367–394, 1988.

[7] J. M. Jasinski, B. S. Meyerson, and B. A. Scott. Mechanistic Studies of Chemical Vapor Deposition. *Annu. Rev. Phys. Chem.*, 38:109–140, 1987.

[8] F. G. Celii and J. E. Butler. Diamond Chemical Vapor Deposition. *Annu. Rev. Phys. Chem.*, 42:643–684, 1991.

[9] R. A. Zhitnikov Dmitriev and Yu. A. Dmitriev. Detection of free radicals in low-temperature gas-grain reactions of astrophysical interest. *Astron. Astrophys.*, 386:1129–1138, 2002.

[10] H. Feuchtgruber, J. I. Moses, and T. Encrenaz. Detection of methyl radicals (CH_3) on Saturn. *Astron. Astrophys.*, 334:L41–L44, 1998.

[11] B. Bézard, P. N. Romani, H. Feuchtgruber, and T. Encrenaz. Detection of the Methyl Radical on Neptune. *Astrophys. J.*, 515:868–872, 1999.

[12] H. Feuchtgruber, F. Helmich, Ewine F. van Dishoeck, and C. M. Wright. Detection of Intersteller CH_3. *Astrophys. J.*, 535:L111–L114, 2000.

[13] Thomas B. Settersten, Roger L. Farrow, and Jeffrey A. Gray. Coherent infrared-ultraviolet double-resonance spectroscopy of CH_3. *Chem. Phys. Lett.*, 370:204–210, 2003.

[14] Allen S. Lefohn and George C. Pimentel. Infrared spectrum of Gaseous Methyl Radical by Rapid Scan Spectroscopy. *J. Chem. Phys.*, 57:4028–4037, 1972.

[15] P. L. Holt, K. E. McCurdy, R. B. Weisman, J. S. Adams, and P. S. Engel. Transient CARS spectroscopy of the ν_1 band of methyl radical. *J. Chem. Phys.*, 81:3349–3350, 1984.

[16] P. B. Kelly and Sion G. Westre. Resonance Raman spectroscopy of the methyl radical. *Chem. Phys. Lett.*, 151:253–257, 1988.

[17] Nancy E. Triggs, Mansour Zahedi, Joseph W. Nibler, Peter DeBarber, and James J. Valentini. High resolution study of the ν_1 vibration of CH_3 by coherent Raman photofragment spectroscopy. *J. Chem. Phys.*, 96:1822–1831, 1992.

[18] Mansour Zahedi, James A. Harrison, and Joseph W. Nibler. 266 nm CH_3I photodissociation: CH_3 spectra and population distributions by coherent Raman spectroscopy. *J. Chem. Phys.*, 100:4043–4055, 1994.

[19] S. Hädrich, S. Hefter, B. Pfelzer, T. Doerk, P. Jauernik, and J. Uhlenbusch. Determination of the absolute Raman cross section of methyl. *Chem. Phys. Lett.*, 256:83–86, 1996.

[20] S. G. Westre and P. B. Kelly. Examination of CD_3 vibrational structure by resonance Raman spectroscopy. *J. Chem. Phys.*, 90:6977–6979, 1989.

[21] James T. Miller, Katherine A. Burton, R. Bruce Weisman, Wen Xue Wu, and Paul S. Engel. CARS spectroscopy of gas phase CD_3. *Chem. Phys. Lett.*, 158:179–183, 1989.

[22] G. D. Stancu, J. Röpcke, and P. B. Davies. Line strengths and transition dipole moment of the ν_2 fundamental band of the methyl radical. *J. Chem. Phys.*, 122:014306/1–11, 2005.

[23] Jeffrey W. Hudgens, T. G. DiGiuseppe, and M. C. Lin. Two photon resonance enhanced multiphoton ionization spectroscopy and state assignments of the methyl radical. *J. Chem. Phys.*, 79:571–582, 1983.

[24] Trygve Helgaker, Sonia Coriani, Kasper Kristensen, Jeppe Olsen, and Kenneth Ruud. Recent Advances in Wave Function-Based Methods of Molecular-Property Calculations. *Chem. Rev.*, 112:543–631, 2012.

[25] Henry F. Schaefer. Methylene: A paradigm for computational quantum chemistry. *Science*, 231:1100–1107, 1986.

[26] Asger Halkier and Peter R. Taylor. A theoretical investigation of the equilibrium electric dipole moment of ammonia. *Chem. Phys. Lett.*, 285:133–137, 1998.

[27] Oleg L. Polyansky, Katarzyna Bielska, Mélanie Ghysels, Lorenzo Lodi, Nikolai F. Zobov, Joseph T. Hodges, and Jonathan Tennyson. High accuracy CO_2 line intensities determined from theory and experiment. *Phys. Rev. Lett.*, 114:243001/1–5, 2015.

[28] M. Born and R. Oppengeimer. On the Quantum Theory of Molecules. *Ann. Phys.*, 84:457–484, 1927.

[29] Philip R. Bunker and Per Jensen. The Born-Oppenheimer Approximation. In Philip R. Bunker and Per Jensen, editors, *Computational Molecular Spectroscopy*, chapter 1, pages 1–11. John Wiley & Sons Ltd, 2000.

[30] P. R. Bunker and R. E. Moss. The breakdown of the Born-Oppenheimer approximation: The effective vibration-rotation hamiltonian for a diatomic molecule. *Mol. Phys.*, 33:417–424, 1977.

[31] Graham A. Worth and Lorenz S. Cederbaum. Beyond Born-Oppenheimer: Molecular Dynamics Through a Conical Intersection. *Annu. Rev. Phys. Chem.*, 55:127–158, 2004.

[32] Wolfgang Demtröder. Breakdown of the Born-Oppenheimer Approximation, Perturbations in Molecular Spectra. In *Molecular Physics: Theoretical Principles and Experimental Methods*, pages 293–323. Wiley-VCH Verlag GmbH, Weinheim, 2005.

[33] Simone Pisana, Michele Lazzeri, Cinzia Casiraghi, Kostya S. Novoselov, A. K. Geim, Andrea C. Ferrari, and Francesco Mauri. Breakdown of the adiabatic Born-Oppenheimer approximation in graphene. *Nature Materials*, 6:198–201, 2007.

[34] Jürgen Gauss and Cristina Puzzarini. Quantum-chemical calculation of Born-Oppenheimer breakdown parameters to rotational constants. *Mol. Phys.*, 108:269–277, 2010.

[35] Igor Rahinov, Russell Cooper, Daniel Matsiev, Christof Bartels, Daniel J. Auerbach, and Alec M. Wodtke. Quantifying the breakdown of the Born-Oppenheimer approximation in surface chemistry. *Phys. Chem. Chem. Phys.*, 13:12680–12692, 2011.

[36] Takehiro Yonehara, Kota Hanasaki, and Kazuo Takatsuka. Fundamental approaches to nonadiabaticity: Toward a chemical theory beyond the Born-Oppenheimer paradigm. *Chem. Rev.*, 112:499–542, 2012.

[37] O. Krechkivska, B. A. Welsh, G. B. Bacskay, K. Nauta, S. H. Kable, and T. W. Schmidt. First observation of the 3 $^3\Pi_g$ state of C_2: Born-Oppenheimer breakdown. *J. Chem. Phys.*, 146:134306/1–8, 2017.

[38] B. T. Sutcliffe. The idea of a potential energy surface. *Mol. Phys.*, 104: 715–722, 2006.

[39] Frank Jensen. *Introduction to Computational Chemistry.* John Wiley & Sons Ltd, Chichester, third edition, 2017.

[40] Attila G. Császár, Csaba Fábri, Tamás Szidarovszky, Edit Mátyus, Tibor Furtenbacher, and Gábor Czakó. The fourth age of quantum chemistry: molecules in motion. *Phys. Chem. Chem. Phys.*, 14:1085–1106, 2012.

[41] Per Jensen. Calculation of Molecular Rotation-Vibration Energies Directly from the Potential Energy Function. In Stephen Wilson and Geerd H F Diercksen, editors, *Methods in Computational Molecular Physics*, pages 423–469. Springer US, Boston, MA, 1992.

[42] Ian M. Mills. Vibration-Rotation Structure in Asymmetric- and Symmetric-Top Molecules. In K. Narahari Rao and C. Weldon Mathews, editors, *Molecular Spectroscopy: Modern Research*, pages 115–140. Academic Press, London, 1972.

[43] D. Papousek and M.R. Aliev. *Molecular Vibrational-Rotational Spectra*. Elsevier Scientific, Amsterdam, 1982.

[44] M. R. Aliev and J. K. G. Watson. Higher-Order Effects in the Vibration-Rotation Spectra of Semirigid Molecules. In K Narahari Rao, editor, *Molecular Spectroscopy: Modern Research*, pages 1–67. Academic Press, London, 1985.

[45] Kamil Sarka and Jean Demaison. Peturbation Theory, Effective Hamiltonians and Force Constanrs. In Per Jensen and Philip R. Bunker, editors, *Computational Molecular Spectroscopy*, chapter 8, pages 255–303. John Wiley & Sons Ltd, Chichester, 2000.

[46] Vincenzo Barone, Julien Bloino, Ciro A Guido, and Filippo Lipparini. A fully automated implementation of VPT2 Infrared intensities. *Chem. Phys. Lett.*, 496:157–161, 2010.

[47] W. James Morgan, Devin A. Matthews, Magnus Ringholm, Jay Agarwal, Justin Z. Gong, Kenneth Ruud, Wesley D. Allen, John F. Stanton, and Henry F. Schaefer. Geometric Energy Derivatives at the Complete Basis Set Limit: Application to the Equilibrium Structure and Molecular Force Field of Formaldehyde. *J. Chem. Theory Comput.*, 14:1333–1350, 2018.

[48] John F. Stanton. Semiclassical Transition-State Theory Based on Fourth-Order Vibrational Perturbation Theory: The Symmetrical Eckart Barrier. *J. Phys. Chem. Lett.*, 7:2708–2713, 2016.

[49] Jonathan Tennyson. Variational Calculations of Rotation–Vibration Spectra. In Per Jensen and Philip R. Bunker, editors, *Computational Molecular Spectroscopy*, pages 305–323. John Wiley & Sons Ltd, Chichester, 2000.

[50] Joel M. Bowman, Tucker Carrington, and Hans Dieter Meyer. Variational quantum approaches for computing vibrational energies of polyatomic molecules. *Mol. Phys.*, 106:2145–2182, 2008.

[51] Ove Christiansen. Selected new developments in vibrational structure theory: potential construction and vibrational wave function calculations. *Phys. Chem. Chem. Phys.*, 14:6672–6687, 2012.

[52] P. Bryan Changala and Joshua H. Baraban. Ab initio effective rotational and rovibrational Hamiltonians for non-rigid systems via curvilinear second order vibrational Moller-Plesset perturbation theory. *J. Chem. Phys.*, 145: 174106/1–13, 2016.

[53] Sergei N. Yurchenko, Miguel Carvajal, Per Jensen, Hai Lin, Jingjing Zheng, and Walter Thiel. Rotation–vibration motion of pyramidal XY_3 molecules described in the Eckart frame: Theory and application to NH_3. *Mol. Phys.*, 103:359–378, 2005.

[54] Sergei N. Yurchenko, Walter Thiel, and Per Jensen. Theoretical ROVibrational Energies (TROVE): A robust numerical approach to the calculation of rovibrational energies for polyatomic molecules. *J. Mol. Spectrosc.*, 245: 126–140, 2007.

[55] Andrey Yachmenev and Sergei N. Yurchenko. Automatic differentiation method for numerical construction of the rotational-vibrational Hamiltonian as a power series in the curvilinear internal coordinates using the Eckart frame. *J. Chem. Phys.*, 143:014105/1–16, 2015.

[56] Sergei N. Yurchenko, Andrey Yachmenev, and Roman I. Ovsyannikov. Symmetry-Adapted Ro-vibrational Basis Functions for Variational Nuclear Motion Calculations: TROVE Approach. *J. Chem. Theory Comput.*, 13: 4368–4381, 2017.

[57] Ahmed F. Al-Refaie, Sergei N. Yurchenko, and Jonathan Tennyson. GPU Accelerated Intensities MPI (GAIN-MPI): A new method of computing Einstein-A coefficients. *Comput. Phys. Commun.*, 214:216–224, 2017.

[58] C. Eckart. Some Studies Concerning Rotating Axes and Polyatomic Molecules. *Phys. Rev.*, 47:552–558, 1935.

[59] Philip R. Bunker and Per Jensen. *Molecular Symmetry and Spectroscopy.* NRC Research Press, Ottawa, second edition, 1998.

[60] André Nauts and Xavier Chapuisat. Momentum, quasi-momentum and hamiltonian operators in terms of arbitrary curvilinear coordinates, with special emphasis on molecular hamiltonians. *Mol. Phys.*, 55:1287–1318, 1985.

[61] Georg Ole Sørensen. A new approach to the Hamiltonian of nonrigid molecules. In *Large Amplitude Motion in Molecules II*, pages 97–175, Berlin, Heidelberg, 1979. Springer Berlin Heidelberg.

[62] B. Kirtman, J. M. Luis, and D. M. Bishop. Simple finite field method for calculation of static and dynamic vibrational hyperpolarizabilities: Curvature contributions. *J. Chem. Phys.*, 108:10008–10012, 1998.

[63] V. E. Ingamells, M. G. Papadopoulos, N. C. Handy, and A. Willetts. The electronic, vibrational and rotational contributions to the dipole moment, polarizability, and first and second hyperpolarizabilities of the BH molecule. *J. Chem. Phys.*, 109:1845–1859, 1998.

[64] B. Kirtman, B. Champagne, and J. M. Luis. Efficient treatment of the effect of vibrations on electrical, magnetic, and spectroscopic properties. *J. Comput. Chem.*, 21:1572–1588, 2000.

[65] V. E. Ingamells, M. G. Papadopoulos, and A. J. Sadlej. Vibrational corrections to properties at arbitrary reference geometry. *J. Chem. Phys.*, 112: 1645–1654, 2000.

[66] P-O Åstrand, K. Ruud, and P. R. Taylor. Calculation of the vibrational wave function of polyatomic molecules. *J. Chem. Phys.*, 112:2655–2667, 2000.

[67] K. Ruud, P-O Åstrand, and P. R. Taylor. An efficient approach for calculating vibrational wave functions and zero-point vibrational corrections to molecular properties of polyatomic molecules. *J. Chem. Phys.*, 112:2668–2683, 2000.

[68] K. Ruud, P.-O. Åstrand, and P. R. Taylor. Vibrational Effects on Molecular Properties in Large Molecules. *Int. J. Comput. Methods Sci. Eng*, 3:7–39, 2003.

[69] T. A. Ruden and K. Ruud. Ro-Vibrational Corrections to NMR Parameters. In Martin Kaupp, Michael Bühl, and Vladimir G. Malkin, editors, *Calculation of NMR and EPR Parameters: Theory and Applications*, pages 153–173. Wiley-VCH Verlag GmbH & Co. KGaA, 2004.

[70] M. Torrent-Sucarrat, J. M. Luis, and B. Kirtman. Variational calculation of vibrational linear and nonlinear optical properties. *J. Chem. Phys.*, 122: 204108/1–10, 2005.

[71] J. M. Luis, H. Reis, M. Papadopoulos, and B. Kirtman. Treatment of nonlinear optical properties due to large amplitude anharmonic vibrational motions: Umbrella motion in NH_3. *J. Chem. Phys.*, 131:034116/1–9, 2009.

[72] C. C. Chou and B. Y. Jin. Vibrational contributions to static linear and nonlinear optical coefficients: from two-level to two-band system. *Theor. Chem. Acc.*, 122:313–324, 2009.

[73] T. B. Pedersen, J. Kongsted, T. D. Crawford, and K. Ruud. On the importance of vibrational contributions to small-angle optical rotation: Fluorooxirane in gas phase and solution. *J. Chem. Phys.*, 130:034310/1–7, 2009.

[74] R. Zaleśny, I. W. Bulik, W. Bartkowiak, J. M. Luis, A. Avramopoulos, M. G. Papadopoulos, and P Krawczyk. Electronic and vibrational contributions to first hyperpolarizability of donor–acceptor-substituted azobenzene. *J. Chem. Phys.*, 133:244308/1–7, 2010.

[75] A. S. Dutra, M. A. Castro, T. L. Fonseca, E. E. Fileti, and S Canuto. Hyperpolarizabilities of the methanol molecule: A CCSD calculation including vibrational corrections. *J. Chem. Phys.*, 132:034307/1–7, 2010.

[76] A. Yachmenev, S. N. Yurchenko, I. Paidarová, P. Jensen, W. Thiel, and S. P. Sauer. Thermal averaging of the indirect nuclear spin-spin coupling constants of ammonia: The importance of the large amplitude inversion mode. *J. Chem. Phys.*, 132:114305/1–15, 2010.

[77] E. S. Naves, M. A. Castro, and T. L. Fonseca. Dynamic (hyper)polarizabilities of the sulphur dioxide molecule: Coupled cluster calculations including vibrational corrections. *J. Chem. Phys.*, 136:014303/1–7, 2012.

[78] M. Garcia-Borrás, M. Solá, D. Lauvergnat, H. Reis, J. M. Luis, and B. Kirtman. A Full Dimensionality Approach to Evaluate the Nonlinear Optical Properties of Molecules with Large Amplitude Anharmonic Tunneling Motion. *J. Chem. Theory Comput.*, 9:520–532, 2013.

[79] X. Chen, Z. Rinkevicius, K. Ruud, and H. Ågren. Role of zero-point vibrational corrections to carbon hyperfine coupling constants in organic pi radicals. *J. Chem. Phys.*, 138:054310/1–8, 2013.

[80] H. Reis, J. M. Luis, M. Garcia-Borrás, and B. Kirtman. Computation of Nonlinear Optical Properties of Molecules with Large Amplitude Anharmonic Motions. III. Arbitrary Double-Well Potentials. *J. Chem. Theory Comput.*, 10:236–242, 2014.

[81] X. Chen, Z. Rinkevicius, Z. Cao, , K. Ruud, and H. Ågren. Zero-point vibrational corrections to isotropic hyperfine coupling constants in polyatomic molecules. *Phys. Chem. Chem. Phys.*, 13:696–707, 2011.

[82] R. D. Wigglesworth, W. T. Raynes, S. P. A. Sauer, and J. Oddershede. Calculated spin–spin coupling surfaces in the water molecule; prediction and analysis of J (O, H), J (O, D) and J (H, D) in water isotopomers. *Mol. Phys.*, 94:851–862, 1998.

[83] J. M. Luis, B. Champagne, and B. Kirtman. Calculation of static zero-point vibrational averaging corrections and other vibrational curvature contributions to polarizabilities and hyperpolarizabilities using field-induced coordinates. *Int. J. Quantum Chem.*, 80:471–479, 2000.

[84] David M. Bishop. Molecular Vibration and Nonlinear Optics. In I. Prigogine and Stuart A. Rice, editors, *Advances in Chemical Physics*, volume 104, pages 1–40. John Wiley & Sons, Inc., 1998.

[85] J. Lounila, R. Wasser, and P. Diehl. Effects of anharmonic vibrations on molecular properties. *Mol. Phys.*, 62:19–31, 1987.

[86] A. J. Russell and M. A. Spackman. Vibrational averaging of electrical properties. *Mol. Phys.*, 84:1239–1255, 1995.

[87] M. H. Beck, A. Jäckle, G. A. Worth, and H.-D. Meyer. The multiconfiguration time-dependent Hartree (MCTDH) method: a highly efficient algorithm for propagating wavepackets. *Phys. Rep.*, 324:1–105, 2000.

[88] J. M. Bowman, S. Carter, and X. C. Huang. MULTIMODE: a code to calculate rovibrational energies of polyatomic molecules. *Int. J. Quantum Chem.*, 22:533–549, 2003.

[89] E. Mátyus, G. Czakó, and A. G. Császár. Toward black-box-type full- and reduced-dimensional variational (ro)vibrational computations. *J. Chem. Phys.*, 130:134112/1–16, 2009.

[90] O. Christiansen. Response theory for vibrational wave functions. *J. Chem. Phys.*, 122:194105/1–9, 2005.

[91] O. Christiansen, J. Kongsted, M. J. Paterson, and J. M. Luis. Linear response functions for a vibrational configuration interaction state. *J. Chem. Phys.*, 125:214309/1–12, 2006.

[92] Gerhard Herzberg. *The Spectra and Structures of Simple Free Radicals: An introduction to molecular spectroscopy.* Cornell University Press, Ithaca, 1st edition, 1971.

[93] W. A. Lathan, W. J. Hehre, L. A. Curtiss, and J. A. Pople. Molecular orbital theory of the electronic structure of organic compounds. X. Systematic study of geometries and energies of AH_n molecules and cations. *J. Am. Chem. Soc.*, 93:6377–6387, 1971.

[94] G. T. Surratt and W. A. Goddard III. Theoretical studies of CH_3, CH_3^+ and CH_3^- using correlated wavefunctions. *Chem. Phys.*, 23:39–50, 1977.

[95] D. S. Marynick and D. A. Dixon. Electron affinity of the methyl radical: Structures of CH_3 and CH_3^-. *Proc. Natl. Acad. Sci.*, 74:410–413, 1977.

[96] V. Špirko and P. R. Bunker. The potential function and rotation-vibration energy levels of the methyl radical CH_3. *J. Mol. Spectrosc.*, 95:381–390, 1982.

[97] Daniel M. Chipman. Theoretical study of the properties of methyl radical. *J. Chem. Phys.*, 78:3112–3132, 1983.

[98] P. Botschwina, J. Flesch, and W. Meyer. Spectroscopic properties of the methyl radical calculated from UHF SCEP wavefunctions. *Chem. Phys.*, 74: 321–338, 1983.

[99] U. Salzner and P. v. R. Schleyer. A successful ab initio study of the adiabatic electron affinity of the methyl radical. *Chem. Phys. Lett.*, 199:267–274, 1992.

[100] D. A. Dixon, D. Feller, and K. A. Peterson. Accurate Calculations of the Electron Affinity and Ionization Potential of the Methyl Radical. *J. Phys. Chem. A*, 101:9405–9409, 1997.

[101] O. Roberto-Neto, S. Chakravorty, and F. B. C. Machado. Coupled–cluster study of the equilibrium geometry and harmonic vibrational frequencies of the methyl radical. *Int. J. Quantum Chem.*, 103:649–653, 2005.

[102] Murat Keçeli, Toru Shiozaki, Kiyoshi Yagi, and So Hirata. Anharmonic vibrational frequencies and vibrationally-averaged structures of key species in hydrocarbon combustion: HCO^+, HCO, HNO, HOO, HOO^-, CH_3^+, and CH_3. *Mol. Phys.*, 107:1283–1301, 2009.

[103] David W. Schwenke. A theoretical study of the ro-vibrational spectrum of the X state of CH_3. *Spectrochim. Acta A*, 55:731–738, 1999.

[104] Dmitry M. Medvedev, Lawrence B. Harding, and Stephen K. Gray. Methyl radical: Ab initio global potential surface, vibrational levels and partition function. *Mol. Phys.*, 104:73–81, 2006.

[105] Y. Ellinger, F. Pauzat, V. Barone, J. Douady, and R. Subra. Ab initio study of the vibrational dependence of hyperfine coupling constants in the methyl, silyl, and formaldehyde anion radicals. *J. Chem. Phys.*, 72:6390–6397, 1980.

[106] Vincenzo Barone, Andre Grand, Camilla Minichino, and Robert Subra. Vibrational modulation effects on the hyperfine coupling constants of fluoromethyl radicals. *J. Chem. Phys.*, 99:6787–6798, 1993.

[107] B. Fernández, O. Christiansen, O. Bludsky, P. Jörgensen, and K. V. Mikkelsen. Theory of hyperfine coupling constants of solvated molecules: Applications involving methyl and ClO radicals in different solvents. *J. Chem. Phys.*, 104:629–635, 1996.

[108] T. B. Adler, G. Knizia, and H.-J. Werner. A simple and efficient CCSD(T)-F12 approximation. *J. Chem. Phys.*, 127:221106/1–4, 2007.

[109] Kirk A. Peterson, Thomas B. Adler, and Hans-Joachim Werner. Systematically convergent basis sets for explicitly correlated wavefunctions: The atoms H, He, B-Ne, and Al-Ar. *J. Chem. Phys.*, 128:084102/1–12, 2008.

[110] P. F. Provasi, G. A. Aucar, and S. P. A. Sauer. The effect of lone pairs and electronegativity on the indirect nuclear spin–spin coupling constants in CH_2X (X=CH_2, NH, O, S): Ab initio calculations using optimized contracted basis sets. *J. Chem. Phys.*, 115:1324–1334, 2001.

[111] E. D. Hedegård, J. Kongsted, and S. P. A. Sauer. Optimized Basis Sets for Calculation of Electron Paramagnetic Resonance Hyperfine Coupling Constants: aug-cc-pVTZ-J for the 3d Atoms Sc–Zn. *J. Comp. Theory Comput.*, 7:4077–4087, 2011.

[112] T. B. Adler and H.-J. Werner. Local explicitly correlated coupled-cluster methods: Efficient removal of the basis set incompleteness and domain errors. *J. Chem. Phys.*, 130:241101/1–5, 2009.

[113] S. Ten-No. Initiation of explicitly correlated Slater-type geminal theory. *Chem. Phys. Lett.*, 398:56–61, 2004.

[114] J. G. Hill, K. A. Peterson, G. Knizia, and H.-J. Werner. Extrapolating MP2 and CCSD explicitly correlated correlation energies to the complete basis set limit with first and second row correlation consistent basis sets. *J. Chem. Phys.*, 131:194105/1–13, 2009.

[115] K. E. Yousaf and K. A. Peterson. Optimized auxiliary basis sets for explicitly correlated methods. *J. Chem. Phys.*, 129:184108/1–7, 2008.

[116] F. Weigend. A fully direct RI-HF algorithm: Implementation, optimised auxiliary basis sets, demonstration of accuracy and efficiency. *Phys. Chem. Chem. Phys.*, 4:4285–4291, 2002.

[117] C. Hättig. Optimization of auxiliary basis sets for RI-MP2 and RI-CC2 calculations: Core-valence and quintuple-zeta basis sets for H to Ar and QZVPP basis sets for Li to Kr. *Phys. Chem. Chem. Phys.*, 7:59–66, 2005.

[118] Hans Joachim Werner, Peter J. Knowles, Gerald Knizia, Frederick R. Manby, and Martin Schütz. Molpro: A general-purpose quantum chemistry program package. *Wiley Interdisciplinary Reviews: Computational Molecular Science*, 2:242–253, 2012.

[119] H. Lin, W. Thiel, S. N. Yurchenko, M. Carvajal, and P. Jensen. Vibrational energies for NH_3 based on high level ab initio potential energy surfaces. *J. Chem. Phys.*, 117:11265–11276, 2002.

[120] Ahmad Y. Adam, Andrey Yachmenev, Sergei N. Yurchenko, and Per Jensen. Ro-vibrational averaging of the isotropic hyperfine coupling constant for the methyl radical. *J. Chem. Phys.*, 143:244306/1–7, 2015.

[121] J. F. Stanton, J. Gauss, L. Cheng, M. E. Harding, D. A. Matthews, and P. G. Szalay. CFOUR, Coupled-Cluster techniques for Computational Chemistry, a quantum-chemical program package. With contributions from A.A. Auer, R.J. Bartlett, U. Benedikt, C. Berger, D.E. Bernholdt, Y.J. Bomble, O. Christiansen, F. Engel, R. Faber, M. Heckert, O. Heun, M. Hilgenberg, C. Huber, T.-C. Jagau, D. Jonsson, J. Jusélius, T. Kirsch, K. Klein, W.J. Lauderdale, F. Lipparini, T. Metzroth, L.A. Mück, D.P. O'Neill, D.R. Price, E. Prochnow, C. Puzzarini, K. Ruud, F. Schiffmann, W. Schwalbach, C. Simmons, S. Stopkowicz, A. Tajti, J. Vázquez, F. Wang, J.D. Watts and the integral packages MOLECULE (J. Almlöf and P.R. Taylor), PROPS (P.R. Taylor), ABACUS (T. Helgaker, H.J. Aa. Jensen, P. Jørgensen, and J. Olsen), and ECP routines by A. V. Mitin and C. van Wüllen. For the current version, see http://www.cfour.de.

[122] S. N. Yurchenko, M. Carvajal, W. Thiel, and P. Jensen. Ab initio dipole moment and theoretical rovibrational intensities in the electronic ground state of PH_3. *J. Mol. Spectrosc.*, 239:71–87, 2006.

[123] S. N. Yurchenko, M. Carvajal, H. Lin, J. J. Zheng, W. Thiel, and P. Jensen. Dipole moment and rovibrational intensities in the electronic ground state of NH_3: Bridging the gap between ab initio theory and spectroscopic experiment. *J. Chem. Phys.*, 122:104317/1–14, 2005.

[124] S. N. Yurchenko, R. J. Barber, A. Yachmenev, W. Thiel, P. Jensen, and J. Tennyson. A variationally computed T=300 K line list for NH_3. *J. Phys. Chem. A*, 113:11845–11855, 2009.

[125] Chikashi Yamada, Eizi Hirota, and Kentarou Kawaguchi. Diode laser study of the ν_2 band of the methyl radical. *J. Chem. Phys.*, 75:5256–5264, 1981.

[126] Scott Davis, David T. Anderson, Geoffrey Duxbury, and David J. Nesbitt. Jet-cooled molecular radicals in slit supersonic discharges: Sub-Doppler infrared studies of methyl radical. *J. Chem. Phys.*, 107:5661–5675, 1997.

[127] Marilyn E Jacox. *Vibrational and Electronic Energy Levels of Polyatomic Transient Molecules*. American Chemical Society, New York, 1 edition, 1994.

[128] Z. Rinkevicius, L. Telyatnyk, O. Vahtras, and H. Ågren. Density functional theory for hyperfine coupling constants with the restricted-unrestricted approach. *J. Chem. Phys.*, 121:7614–7623, 2004.

[129] E. D. Hedegård, J. Kongsted, and S. P. A. Sauer. Improving the calculation of electron paramagnetic resonance hyperfine coupling tensors for d-block metals. *Phys. Chem. Chem. Phys.*, 14:10669–10676, 2012.

[130] E. D. Hedegård, J. Kongsted, and S. P. A. Sauer. Validating and Analyzing EPR Hyperfine Coupling Constants with Density Functional Theory. *J. Chem. Theory Comput.*, 7:2380–2388, 2013.

[131] Richard W. Fessenden. Electron spin resonance spectra of some substituted methyl radicals. *J. Phys. Chem.*, 71:74–83, 1967.

[132] Chikashi Yamada and Eizi Hirota. The transition dipole moment of the ν_2 band of the methyl radical. *J. Chem. Phys.*, 78:669–671, 1983.

[133] J. Wormhoudt and K. E. McCurdy. A measurement of the strength of the ν_2 band of CH_3. *Chem. Phys. Lett.*, 156:47–50, 1989.

[134] Gabi D. Stancu, Jürgen Röpcke, and Paul B. Davies. Measurement of the Transition Dipole Moment of the First Hot Band of the ν_2 Mode of the Methyl Radical by Diode Laser Spectroscopy. *J. Phys. Chem. A*, 112:6285–6288, 2008.

[135] Gerhard Herzberg. *Molecular Spectra and Molecular Structure: II. Infrared and Raman Spectra of Polyatomic Molecules.* D. Van Nostrand Co. Inc., New York, 1st edition, 1945.

[136] G. D. Purvis and R. J. Bartlett. A full coupled-cluster singles and doubles model the inclusion of disconnected triples. *J. Chem. Phys.*, 76:1910–1918, 1982.

[137] K. Raghavachari, G. W. Trucks, J. A. Pople, and M. Head-Gordon. A fifth-order perturbation comparison of electron correlation theories. *Chem. Phys. Lett.*, 157:479–483, 1989.

[138] T. H. Dunning. Gaussian basis sets for use in correlated molecular calculations. I. The atoms boron through neon and hydrogen. *J. Chem. Phys.*, 90: 1007–1023, 1989.

[139] D. E. Woon and T. H. Dunning. Gaussian basis sets for use in correlated molecular calculations. III. The atoms aluminum through argon. *J. Chem. Phys.*, 98:1358–1371, 1993.

[140] Sergei N. Yurchenko, Walter Thiel, Miguel Carvajal, Hai Lin, and Per Jensen. Rotation-Vibration Motion of Pyramidal XY_3 Molecules Described in the Eckart Frame: The Calculation of Intensities with Application to NH_3. *Adv. Quantum Chem.*, 48:209–238, 2005.

[141] Philip R. Bunker and Per Jensen. *The Fundamentals of Molecular Symmetry.* CRC Press, Boca Raton, first edition, 2004.

[142] Roman I. Ovsyannikov, Walter Thiel, Sergei N. Yurchenko, Miguel Carvajal, and Per Jensen. Vibrational energies of PH_3 calculated variationally at the complete basis set limit. *J. Chem. Physics*, 129:044309/1–8, 2008.

[143] Ahmad Y. Adam, Andrey Yachmenev, Sergei N. Yurchenko, and Per Jensen. Variationally computed IR line list for the methyl radical CH_3. *J. Phys. Chem. A*, 123:4755–4763, 2019.

[144] Heinz W. Hermann and Stephen R. Leone. Photofragmentation dynamics of CH_3I at 248 and 266 nm: Vibrational distributions in the $CH_3(\nu_2)$ "umbrella" mode. *J. Chem. Phys.*, 76:4766–4774, 1982.

[145] S. N. Yurchenko, A. F. Al-Refaie, and J. Tennyson. ExoCross: a general program for generating spectra from molecular line lists. *Astron. Astrophys.*, 614:A131/1–12, 2018.

[146] B. P. Mant, A. Yachmenev, J. Tennyson, and S. N. Yurchenko. ExoMol molecular line lists - XXVII: spectra of C_2H_4. *Mon. Not. R. Astr. Soc.*, 478: 3220–3232, 2018.

[147] Jonathan Tennyson, Sergei N. Yurchenko, Ahmed F. Al-Refaie, Emma J. Barton, Katy L. Chubb, Phillip A. Coles, S. Diamantopoulou, Maire N. Gorman, Christian Hill, Aden Z. Lam, Lorenzo Lodi, Laura K. McKemmish, Yueqi Na, Alec Owens, Oleg L. Polyansky, Tom Rivlin, Clara Sousa-Silva, Daniel S. Underwood, Andrey Yachmenev, and Emil Zak. The ExoMol database: Molecular line lists for exoplanet and other hot atmospheres. *J. Mol. Spectrosc.*, 327:73–94, 2016.

[148] G. A. Bethardy and R. Glen Macdonald. Direct measurement of the transition dipole moment of the ν_3 asymmetric C-H stretching vibration of the CH_3 radical. *J. Chem. Phys.*, 103:2863–2872, 1995.

[149] I. Tanarro, M. M. Sanz, C. Domingo, D. Bermejo, J. Santos, and J. L. Domenech. Transition Dipole Moment of the ν_3 Band of CH_3. *J. Phys. Chem.*, 98:5862–5866, 1994.

[150] Ahmad Y. Adam, Per Jensen, Andrey Yachmenev, and Sergei N. Yurchenko. Nonresonant Raman spectra of the methyl radical $^{12}CH_3$ simulated in variational calculations. *J. Mol. Spectrosc.*, 362:77–83, 2019.

[151] Lorenzo Lodi and Jonathan Tennyson. Theoretical methods for small-molecule ro-vibrational spectroscopy. *J. Phys. B: At. Mol. Opt. Phys.*, 43: 133001/1–44, 2010.

[152] M. Skulinova, C. Lefebvre, P. Sobron, E. Eshelman, M. Daly, J. F. Gravel, J. F. Cormier, F. Châteauneuf, G. Slater, W. Zheng, A. Koujelev, and R. Léveillé. Time-resolved stand-off UV-Raman spectroscopy for planetary exploration. *Planet. Space Sci.*, 92:88–100, 2014.

[153] William J. Abbey, Rohit Bhartia, Luther W. Beegle, Lauren DeFlores, Veronica Paez, Kripa Sijapati, Shakher Sijapati, Kenneth Williford, Michael Tuite, William Hug, and Ray Reid. Deep UV Raman spectroscopy for planetary exploration: The search for in situ organics. *Icarus*, 290:201–214, 2017.

[154] David J. Swanton, George B. Bacskay, and Noel S. Hush. An ab initio SCF calculation of the polarizability tensor, polarizability derivatives and Raman scattering activities of the water-dimer molecule. *Chem. Phys.*, 83: 69–75, 1984.

[155] R. D. Amos. Calculation of polarizability derivatives using analytic gradient methods. *Chem. Phys. Lett.*, 124:376–381, 1986.

[156] O. Quinet and B. Champagne. Time-dependent Hartree-Fock schemes for analytical evaluation of the Raman intensities. *J. Chem. Phys.*, 115:6293–6299, 2001.

[157] C. van Caillie and R. D. Amos. Raman intensities using time dependent density functional theory. *Phys. Chem. Chem. Phys.*, 2:2123–2129, 2000.

[158] Dmitrij Rappoport and Filipp Furche. Lagrangian approach to molecular vibrational Raman intensities using time-dependent hybrid density functional theory. *J. Chem. Phys.*, 126:201104/1–5, 2007.

[159] L. Jensen, J. Autschbach, M. Krykunov, and G. C. Schatz. Resonance vibrational Raman optical activity: A time-dependent density functional theory approach. *J. Chem. Phys.*, 127:134101/1–11, 2007.

[160] Magdalena Pecul and Antonio Rizzo. Linear response coupled cluster calculation of Raman scattering cross sections. *J. Chem. Phys.*, 116:1259–1268, 2002.

[161] Johannes Neugebauer, Markus Reiher, and Bernd A. Hess. Coupled-cluster Raman intensities: Assessment and comparison with multiconfiguration and density functional methods. *J. Chem. Phys.*, 117:8623–8633, 2002.

[162] Magdalena Pecul and Sonia Coriani. The effect of triple excitations in coupled cluster calculations of Raman scattering cross-sections. *Chem. Phys. Lett.*, 355:327–338, 2002.

[163] Darragh P. O'Neill, Mihály Kállay, and Jürgen Gauss. Analytic evaluation of Raman intensities in coupled-cluster theory. *Mol. Phys.*, 105:2447–2453, 2007.

[164] Magdalena Pecul and Antonio Rizzo. Relativistic effects on the electric polarizabilities and their geometric derivatives for hydrogen halides and dihalogens – a Dirac–Hartree–Fock study. *Chem. Phys. Lett.*, 370:578–588, 2003.

[165] Luciano N. Vidal and Pedro A. M. Vazquez. Frequency dependent Raman scattering activities of BeH_2, MgH_2, CaH_2, SrH_2, and H_2O, H_2S, H_2Se, H_2Te, evaluated by the ab initio relativistic four component method Dirac–Hartree–Fock. *Chem. Phys.*, 321:209–214, 2006.

[166] Lorenzo Maschio, Bernard Kirtman, Michel Rérat, Roberto Orlando, and Roberto Dovesi. Ab initio analytical Raman intensities for periodic systems through a coupled perturbed Hartree-Fock/Kohn-Sham method in an atomic orbital basis. I. Theory. *J. Chem. Phys.*, 139:164101/1–13, 2013.

[167] Magnus Ringholm, Radovan Bast, Luca Oggioni, Ulf Ekström, and Kenneth Ruud. Analytic calculations of hyper-Raman spectra from density functional theory hyperpolarizability gradients. *J. Chem. Phys.*, 141:134107/1–10, 2014.

[168] Lasse Jensen, Christine M. Aikens, and George C. Schatz. Electronic structure methods for studying surface-enhanced Raman scattering. *Chem. Soc. Rev.*, 37:1061–1073, 2008.

[169] Václav Parchaňský, Josef Kapitán, and Petr Bouř. Inspecting chiral molecules by Raman optical activity spectroscopy. *RSC Adv.*, 4:57125–57136, 2014.

[170] Kenneth. Ruud and Andreas J. Thorvaldsen. Theoretical Approaches to the Calculation of Raman Optical Activity Spectra. *Chirality*, 21:E54–E67, 2009.

[171] T. Daniel Crawford and Kenneth Ruud. Coupled-cluster calculations of vibrational Raman optical activity spectra. *Chem. Phys. Chem.*, 12:3442–3448, 2011.

[172] Jaroslav Šebestík and Petr Bouř. Observation of paramagnetic Raman optical activity of nitrogen dioxide. *Angew. Chem. Int. Ed.*, 53:9236–9239, 2014.

[173] Dhabih V Chulhai and Lasse Jensen. Simulating Surface-Enhanced Raman Optical Activity Using Atomistic Electrodynamics-Quantum Mechanical Models. *J. Phys. Chem. A*, 118:9069–9079, 2014.

[174] Benjamin G. Janesko and Gustavo E. Scuseria. Surface enhanced Raman optical activity of molecules on orientationally averaged substrates: Theory of electromagnetic effects. *J. Chem. Phys.*, 125:124704/1–12, 2006.

[175] Vít Novák, Jaroslav Šebestík, and Petr Bouř. Theoretical modeling of the surface-enhanced raman optical activity. *J. Chem. Theory Comput.*, 8:1714–1720, 2012.

[176] Dmitrij Rappoport, Sangwoo Shim, and Alán Aspuru-Guzik. Simplified sum-over-states approach for predicting resonance raman spectra. Application to nucleic acid bases. *J. Phys. Chem. Lett.*, 2:1254–1260, 2011.

[177] Julien Guthmuller. Assessment of TD-DFT and CC2 methods for the calculation of resonance raman intensities: Application to o-nitrophenol. *J. Chem. Theory Comput.*, 7:1082–1089, 2011.

[178] Daniel W. Silverstein, Niranjan Govind, Hubertus J. J. van Dam, and Lasse Jensen. Simulating One-Photon Absorption and Resonance Raman Scattering Spectra Using Analytical Excited State Energy Gradients within Time-Dependent Density Functional Theory. *J. Chem. Theory Comput.*, 9:5490–5503, 2013.

[179] Alberto Baiardi, Julien Bloino, and Vincenzo Barone. Accurate Simulation of Resonance-Raman Spectra of Flexible Molecules: An Internal Coordinates Approach. *J. Chem. Theory Comput.*, 11:3267–3280, 2015.

[180] Zu Yong Gong, Guangjun Tian, Sai Duan, and Yi Luo. Significant Contributions of the Albrecht's A Term to Nonresonant Raman Scattering Processes. *J. Chem. Theory Comput.*, 11:5385–5390, 2015.

[181] R. N. Zare. *Angular Momentum: Understanding Spatial Aspects in Chemistry and Physics*. John Wiley and Sons, New York, 1988.

[182] G. Placzek. Rayleigh-Streuung und Raman-Effekt. In E. Marx, editor, *Handbuch der Radiologie*, volume 6, pages 205–374. Academische Verlag, Leipzig, 1934.

[183] Alan Snelson. Infrared matrix isolation spectrum of the methyl radical produced by pyrolysis of methyl iodide and dimethyl mercury. *J. Phys. Chem.*, 74:537–544, 1970.

[184] J. Pacansky, W. Koch, and M. D. Miller. Analysis of the Structures, Infrared Spectra, and Raman Spectra for the Methyl, Ethyl, Isopropyl, and tert-Butyl Radicals. *J. Am. Chem. Soc.*, 113:317–328, 1991.

[185] S. Ajith Perera, John D. Watts, and Rodney J. Bartlett. A theoretical study of hyperfine coupling constants. *J. Chem. Phys.*, 100:1425–1434, 1994.